NEUROSCIENCE

AntimiR treatment corrects myotonic dystrophy primary cell defects across several CTG repeat expansions with a dual mechanism of action

Estefanía Cerro-Herreros[1,2,3], Judit Núñez-Manchón[4], Neia Naldaiz-Gastesi[5,6], Marc Carrascosa-Sàez[3]†, Andrea García-Rey[1,2], Diego Piqueras Losilla[3], Irene González-Martínez[1,2,7], Jorge Espinosa-Espinosa[1,2,7,8], Kevin Moreno[3], Javier Poyatos-García[9,10], Juan J. Vilchez[9,10,11], Adolfo López de Munain[5,6,12,13], Mònica Suelves[4], Gisela Nogales-Gadea[4], Beatriz Llamusí[3], Rubén Artero[1,2,7]*

This study evaluated therapeutic antimiRs in primary myoblasts from patients with myotonic dystrophy type 1 (DM1). DM1 results from unstable CTG repeat expansions in the *DMPK* gene, leading to variable clinical manifestations by depleting muscleblind-like splicing regulator protein MBNL1. AntimiRs targeting natural repressors miR-23b and miR-218 boost MBNL1 expression but must be optimized for a better pharmacological profile in humans. In untreated cells, miR-23b and miR-218 were up-regulated, which correlated with CTG repeat size, supporting that active MBNL1 protein repression synergizes with the sequestration by CUG expansions in *DMPK*. AntimiR treatment improved RNA toxicity readouts and corrected regulated exon inclusions and myoblast defects such as fusion index and myotube area across CTG expansions. Unexpectedly, the treatment also reduced *DMPK* transcripts and ribonuclear foci. A leading antimiR reversed 68% of dysregulated genes. This study highlights the potential of antimiRs to treat various DM1 forms across a range of repeat sizes and genetic backgrounds by mitigating MBNL1 sequestration and enhancing protein synthesis.

INTRODUCTION

Myotonic dystrophy type 1 (DM1) is a rare neuromuscular disease caused by an expansion of a CTG microsatellite repeat in the 3′ untranslated region of the DM1 protein kinase (*DMPK*) gene (*1*). The expansion size may reach thousands of CTG triplets in patients with DM1, compared to 5 to 37 in the general unaffected population. The disease has a prevalence of 1 of 3000 to 1 of 8000 individuals worldwide (*2*), making it the most common muscular dystrophy in adults. The length of the CTG tract in peripheral blood roughly correlates with disease severity, survival, and age of onset (*3*). According to this, several clinical forms are described: congenital, infantile, juvenile, adult, and late-onset DM1 (*4*). A variable multisystem array of symptoms characterizes the disease due to the widespread ubiquitous expression of the *DMPK* gene, particularly cardiac conduction problems, skeletal muscle atrophy, and myotonia. Patient's sex is also a modifying factor influencing DM1 phenotype (*5*).

DMPK transcripts containing expanded CUG triplets accumulate in the nucleus and induce toxicity by affecting RNA processing mechanisms and disturbing key cell signaling pathways (*2*, *6*). A chief molecular event contributing to DM1 pathogenesis involves the expansion size-dependent sequestration of muscleblind-like (MBNL) splicing regulator proteins in mutant *DMPK* transcripts, mainly MBNL1 in skeletal muscles, forming nuclear aggregates called foci (*7*). MBNL1 sequestration affects the functional steady-state levels of the protein, depleting it from the nucleus and impairing its functions as a regulator of pre-mRNA alternative splicing and polyadenylation (*8*–*10*). Stress responses triggered by the accumulation of toxic *DMPK* RNA in the cell nucleus also cause the activation of MBNL1 antagonists, such as CELF1 (*11*), Staufen1 (*12*), and hnRNPA1 (*13*). Together, these proteins function as developmental regulators, and their imbalance in DM1 causes abnormal persistence of fetal patterns of alternative splicing and other pre-mRNA processing defects in adult tissues. This pathological mechanism affects hundreds of genes in several tissues and organs, many of which have been directly connected to some pathological manifestations in DM1. For example, abnormal splicing of *cTNT*, *CLCN1*, and *INSR* have been respectively linked to cardiac conduction problems (*14*), myotonia (*15*), and insulin resistance (*16*).

The length of the CTG repeats changes over time in different cells and tissues (*17*), with a strong tendency toward generating expanded alleles (*18*). In tissues relevant to DM1 pathology, much larger expansions are found in skeletal muscles and the heart, compared to peripheral blood (*19*). This phenomenon largely explains the age-dependent and variable nature of DM1 symptoms and has crucial

[1]Human Translational Genomics Group. University Research Institute for Biotechnology and Biomedicine (BIOTECMED), Universidad de Valencia, 46100 Burjassot, Valencia, Spain. [2]INCLIVA Biomedical Research Institute, Avenue Menéndez Pelayo 4 acc, 46010 Valencia, Spain. [3]ARTHEx Biotech, Parque Científico de la Universidad de Valencia. Calle del Catedrático Agustín Escardino Benlloch, 9, 46980 Paterna, Valencia, Spain. [4]Group of REsearch Neuromuscular of BAdalona (GRENBA), Institut d'Investigació en Ciències de la Salut Germans Trias i Pujol (IGTP), Campus Can Ruti, Universitat Autònoma de Barcelona, 08916 Badalona, Spain. [5]Neuromuscular Diseases Group, Neurosciences Area, Biodonostia Health Research Institute, 20014 Donostia/San Sebastián, Spain. [6]CIBERNED, Carlos III Institute, Spanish Ministry of Science and Innovation, Madrid, Spain. [7]Centre for Biomedical Network Research on Rare Diseases (CIBERER), CB23/07/00005, Carlos III Health Institute, 28029 Madrid, Spain. [8]Experimental and Applied Biomedicine Research Group, Health Sciences Faculty, Universidad Particular Internacional SEK (UISEK), Quito 170302, Ecuador. [9]Neuromuscular and Ataxias Research Group, Health Research Institute Hospital La Fe (IIS La Fe), Valencia, Spain. [10]Centre for Biomedical Network Research on Rare Diseases (CIBERER), U763, CB06/05/0091, Madrid, Spain. [11]Neuromuscular Referral Center, European Reference Network on Rare Neuromuscular Diseases (ERN EURO-NMD), Universitary and Polytechnic La Fe Hospital, Valencia, Spain. [12]Department of Neurology, Donostialdea Integrated Health Organization, Osakidetza Basque Health Service, 20014 Donostia/San Sebastián, Spain. [13]Department of Neurosciences, Faculty of Medicine and Nursery, University of the Basque Country UPV-EHU, 20014 Donostia/San Sebastián, Spain.
*Corresponding author. Email: ruben.artero@uv.es
†Present address: Institute for Integrative Systems Biology (I2SysBio), University of Valencia—CSIC, Paterna, Valencia 46980, Spain.

implications for clinical management because the mutation size in a blood sample does not adequately predict the pathogenic load in other tissues (*20*), particularly muscle (*21*). In addition, individual genetic background and non-CTG repeat interruptions are also known to impinge on the clinical presentation of the disease (*22*). Thus, muscle cells directly isolated from a diverse cohort of patients constitute a valuable tool to validate novel DM1 therapies in the natural genetic context of the mutation (*23*).

Several therapeutical strategies are under development for DM1 (*24*), including antisense oligonucleotides (AONs) designed to release sequestered MBNLs by either targeting *DMPK* transcripts for degradation or blocking the binding between both (*25*). An alternative approach is using AONs to rescue the normal free levels of MBNL proteins because essential DM1 molecular alterations stem from the depletion of these proteins alone (*25*), which remain encoded in functional genes. From the three human MBNL paralogs, MBNL1 is mainly expressed in skeletal muscles and MBNL2 in the central nervous system, while MBNL3 performs functions associated with regeneration and aging (*26*–*29*). MBNL1 overexpression is well tolerated and prevents typical DM1 alterations (*30*, *31*). From a therapeutic perspective, this is a particularly favorable situation because MBNL1 protein depletion (and antagonist activity) can be compensated with enhanced endogenous expression (*30*, *32*, *33*), which is naturally repressed by miR-23b and miR-218 microRNAs (miRNAs) (*34*). Recently, miRNA-targeting AONs, so-called antimiRs, have been developed to block miR-23b and miR-218, increasing MBNL1 expression and correcting functional and histopathological DM1 alterations (*34*–*36*). These AONs (antimiR-23b-V1 and antimiR-218-V1) were fully modified with 2′-*O*-methyl (2′-OMe) chemistry, including several phosphorothioate (PS) linkages at each end, and were conjugated to cholesterol at the 3′ end.

In the current study, we used eight DM1 primary myoblast cell lines and nine unaffected controls to test the effect of antimiR-23b-V1 and antimiR-218-V1, reported previously (*34*), together with a new generation of chemically modified antimiRs named antimiR-23b-V2 and antimiR-218-V2. V2 molecules incorporate a combination of 2′-OMe, 2′-*O*-methoxyethyl (MOE), and locked nucleic acid (LNA) residues throughout their sequence, and, furthermore, antimiR-23b-V2 and antimiR-218-V2 are conjugated with fatty acid to enhance their biodistribution (*37*). The cells were transfected at two differentiation times to study multiple RNA toxicity readouts, finding that antimiRs enhance MBNL1 protein expression and reduce *DMPK* transcript levels. The results demonstrate that lead antimiR drugs rescue DM1 defects across multiple genetic backgrounds in vitro through a dual mechanism of action.

RESULTS

Characterization of myoblast cell lines from patients with adult- and juvenile-onset DM1

Seven patients with adult-onset DM1 (five females and two males) and one with juvenile-onset DM1 (female) served as donors to derive the myoblast cell lines used in our study (Table 1). The length of the CTG repeat was determined in all cases using DNA from the cells, ranging from 117 to 1054 triplets. Information about repeat length from muscle tissue was available in two cases and closely matched the size observed in vitro: 726/736 and 835/788 (myoblasts/muscle). We also determined the CTG repeat length in blood at the time of biopsy collection. As expected, the number of triplets was lower compared to muscle tissue in all cell lines except MP-10-31.

Variability in the patient's muscle function and disability were clearly shown by the battery of functional tests performed (Table 1), which included the 6-min walking test (6MWT) (*38*), the muscle impairment rating scale (MIRS) (*39*), the modified Rankin scale (mRS) (*40*), and the biceps Medical Research Council (MRC) (*41*). Despite limited data availability and the qualitative nature of the variables (except 6MWT), we observed moderate positive correlations (R between 0.5 and 0.7; P values <0.2) between CTG repeat length in muscle cells and scales of muscle impairment and patient disability (MIRS and mRS, respectively). In contrast, a negative correlation ($R = -0.86$) was observed between CTG repeat length and muscle strength, measured as the MRC score of the biceps (fig. S1). Primary myoblasts from these patients were treated with antimiRs, differentiated, and evaluated for miR-23b and miR-218 levels, MBNL1 expression and subcellular distribution and nuclear foci, RNA foci, *DMPK* mRNA expression, myotube area, and fusion index (fig. S2).

Reduction of miR-23b and miR-218 overexpression during DM1 myotube differentiation by antimiR treatment

We analyzed miR-23b and miR-218 levels in all primary myoblast cell lines as an indication of the expression of these miRNAs before antimiR treatment (Fig. 1, A and B). At 10 days of differentiation, the expression of miR-23b and miR-218 was ~2.5-fold and 5-fold higher in DM1 cells compared to control myoblasts, respectively ($P < 0.05$), a difference that was still not conspicuous by 5 days of differentiation. At both time points, we observed a marked variability in DM1 cells compared to controls. We wondered whether this higher dispersion could be attributed to phenotypic differences caused by the variability in CTG repeat length. In support of this possibility, we observed a significant correlation of CTG repeat length of DM1 myoblasts with miR-23b and miR-218 expressions (fig. S3). On the other hand, receptor operating curve analysis revealed an area under the curve of 82% for miR-23b and 89% for miR-218, indicating that levels of these miRNAs have the potential to predict CTG repeat size in patients accurately (fig. S3).

Upon antimiR-23b-V1 treatment of DM1 myoblasts, we observed a significant 65 to 75% reduction in the detection of miR-23b at day 10 of differentiation for both concentrations (34 and 54 nM). The detection on day 5 was already significantly lower using the 54 nM concentration, but not with the 34 nM dose (Fig. 1C). The miRNA antagonistic activity of antimiR-23b-V2 seems to be considerably stronger since 85 to 95% reduction of miRNA detection was observed at both time points, and it was significantly lower using the 34 nM dose. Regarding miR-218 AONs, antimiR-218-V1 and -V2 performed similarly across both differentiation time points (Fig. 1D). We observed reductions in the detection of miR-218 in the 30 to 75% range, with trends of higher activities at 220 nM compared to 138 nM. Together, these results confirm robust reductions in the detected levels of target miRNAs in all cell lines. In addition, we observed a trend of increased efficacy of antimiR-23b-V2.

Reduction of MBNL1 levels during differentiation of DM1 myotubes and their increase upon antimiR treatment

Alternative splicing of *MBNL1* transcripts helps tailor protein function to actual cell necessities. The inclusion of exon 5 completes a bipartite nuclear localization signal. Consequently, abnormal inclusion

Table 1. Characterization of DM1 and control cell donors that participated in this study. Muscle performance parameters, mutation size of DM1 patient donors used in the study, and muscle origin and age at sampling for both DM1 samples and controls.

ID	Sample type	Sex	Biopsy muscle	Age at sampling (y)	Age of onset (y)	Estimated number of CTG triplets in myoblast/muscle*	Estimated number of CTG triplets in Blood	6MWT† (m)	MIRS‡	mRS§	Biceps MRC¶	Cohort
SP3	DM1 (juvenile onset)	Female	Biceps brachialis	36	15	726/736*	445	348	4	2	4	A
SP6	DM1 (adult onset)	Female	Biceps brachialis	41	36	686	338	368	2	1	5	A
SP10	DM1 (adult onset)	Female	Biceps brachialis	39	27	835/788*	374	N.D.	4	4	4	A
SP12	DM1 (adult onset)	Male	Biceps brachialis	41	36	265	130	519	3	2	5	A
B55	DM1 (adult onset)	Female	Deltoid	47	30	1054	800	N.D.	4	3	4	B
MP-09-57	DM1 (adult onset)	Female	Intrinsic muscles of the hand or forearm	31	30	702	333	N.D.	2	N.D.	N.D.	C
MP-09-73	DM1 (adult onset)	Male	Intrinsic muscles of the hand or forearm	49	20	704	233	N.D.	2	N.D.	N.D.	C
MP-10-31	DM1 (adult onset)	Female	Biceps brachialis	34	15	117	1400	N.D.	3	N.D.	N.D.	C
C5	Control	Female	Intrinsic muscles of the hand or forearm	67	-	-	-	-	-	-	-	A
C7	Control	Female	Intrinsic muscles of the hand or forearm	66	-	-	-	-	-	-	-	A
C9	Control	Male	Intrinsic muscles of the hand or forearm	41	-	-	-	-	-	-	-	A
C10	Control	Male	Intrinsic muscles of the hand or forearm	26	-	-	-	-	-	-	-	A
C11	Control	Female	Intrinsic muscles of the hand or forearm	35	-	-	-	-	-	-	-	A
C12	Control	Male	Intrinsic muscles of the hand or forearm	73	-	-	-	-	-	-	-	A
B71	Control	Male	Medial calf	18	-	-	-	-	-	-	-	B
MP-35	Control	Male	Vastus lateralis	35	-	-	-	-	-	-	-	C
MP-49	Control	Female	Vastus lateralis	49	-	-	-	-	-	-	-	C

†The 6-min walking test (6MWT) is an index of aerobic endurance capacity, distance in meters walked by a patient during 6 min (*38*). ‡Muscle impairment rating scale (MIRS), assesses the degree of distal to proximal muscle involvement (*39*). §Modified Rankin scale (mRS), an indicator of disability in patients (*40*). ¶Biceps Medical Research Council (MRC), scale indicative of muscle strength (*41*). N.D., not determined; A, Germans Trias i Pujol Hospital, Barcelona, Catalonia (Spain); B, La Fe University and Polytechnic Hospital, Valencia, Valencian Community (Spain); C, Donostia University Hospital, San Sebastian, Bask Country (Spain).

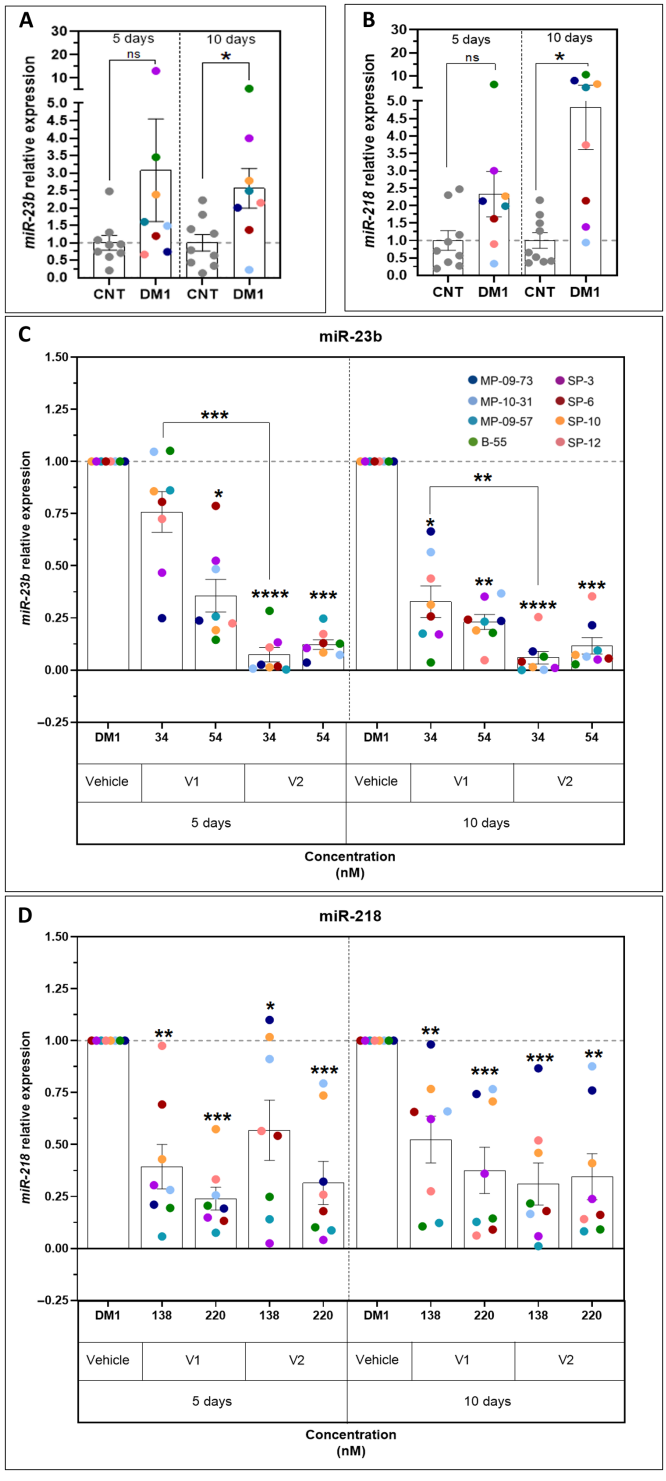

Fig. 1. Expression of target miRNAs in DM1 cells and treatment modulation. The upper graphs show the quantification of (**A**) miR-23b and (**B**) miR-218 expression in control versus DM1 cells during differentiation. Unpaired *t* test with Welch's correction. The bottom graphs show the quantification of (**C**) miR-23b and (**D**) miR-218 expression upon antimiR treatment. Kruskal-Wallis test $*P < 0.05$; $**P < 0.01$; $***P < 0.001$; $****P < 0.0001$ (Dunn's posttest). Each dot of a different color denotes a different DM1 myoblast line. The asterisks above the bars denote DM1 comparisons, while those above the boxes denote dose comparisons. The names of the lines are shown in the legend. Error bars represent the SEM. ns, not significant.

of this exon is expected to enhance the potential of MBNL1 to be sequestered with nuclear CUG expansions, so it can be used as an indicator of the pathogenic status of the cell. As a result of its regulatory splicing activity, MBNL1 promotes the exclusion of its own exon 5 (*42*, *43*).

MBNL1 protein levels were significantly lower in DM1 myotubes after 10 days of differentiation compared to controls, with a trend already noticeable by day 5 (Fig. 2). This pattern was observed for total MBNL1 protein levels (Fig. 2A), MBNL1 42/43 kDa (+ex5 ± ex7) and MBNL1 40/41 kDa (−ex5 ± ex7) isoforms (Fig. 2, B and C). Total and isoform-specific MBNL1 levels were somewhat variable in both the control and DM1 cell cohorts. This was expected because of the combination of several factors such as muscle of origin, sex and age of donors, repeat expansion size, number of in vitro cell passages, and genetic background effects, in addition to the intrinsic experimental variability in all these determinations. Despite all these sources of variability, the average expression levels of total MBNL1 and isoforms 42/43 and 40/41 reached statistical significance. The biological relevance of these changes is reinforced by focusing on total MBNL1 levels, which reached statistical significance not because of lower dispersion of data (SD is actually higher than at 5 days) but because of lower average amounts.

We observed a significant negative correlation between CTG repeat length of DM1 myoblasts and MBNL1 levels, both for total protein and each MBNL1 protein isoform individually (borderline for isoform 40/41 kDa; Fig. 2, D to F). This coincides with the positive correlation between repeat length and miR-23b and miR-218 levels (fig. S3). The ratio between these isoforms changed during the differentiation of DM1 cells (fig. S4). At day 5 of differentiation, we observed a ~60/40 ratio between high/low MW isoforms. By day 10, the ratio changed to ~70/30 in DM1 myotubes but remained ~60/40 in control cells, which is a difference consistent with observations reported by others (*44*).

Upon antimiR treatment, we observed a significant increase in total MBNL1 levels in both differentiation time points using the higher doses of 54 and 220 nM for antimiRs against miR-23b and miR-218, respectively (Fig. 2G). We observed a fourfold increase in total MBNL levels using antimiR-23b-V2. In all cases, the derepression at these doses was significantly higher than at the lower doses of 34 and 138 nM, respectively. Both MBNL1 isoforms contributed to the total increase in protein levels (fig. S5, A and B). AntimiRs brought about a solid dose-dependent up-regulation of total MBNL1 levels, also detectable at the isoform level, in patient-derived primary myoblasts. Significantly, antimiR treatment had a similar effect on the isoform ratio at days 5 and 10 of differentiation in DM1 cells, maintaining about 50 to 55% the percentage of MBNL1 42/43, but because untreated disease controls increased the percentage of this isoform from approximately 60 to 70% at days 5 and 10, respectively, the overall therapeutic activity of antimiRs (measured as skipping of ex5 in *MBNL1*, which is a splicing activity regulated by the protein itself), increased with differentiation time (fig. S5C).

Reduction in the number of RNA and MBNL1 nuclear foci and *DMPK* transcripts upon antimiR treatment

DM1 myotubes presented an average of five to six foci per nucleus, and, as expected (*45*), control cells did not show any (Fig. 3A). AntimiR treatment at higher doses than in our previous reports (*34*) reduced the average number of foci in DM1 cells (Fig. 3B). These reductions were significant for both versions of antimiR-23b and differentiation time points. AntimiR-218-V1 and -V2 also reduced

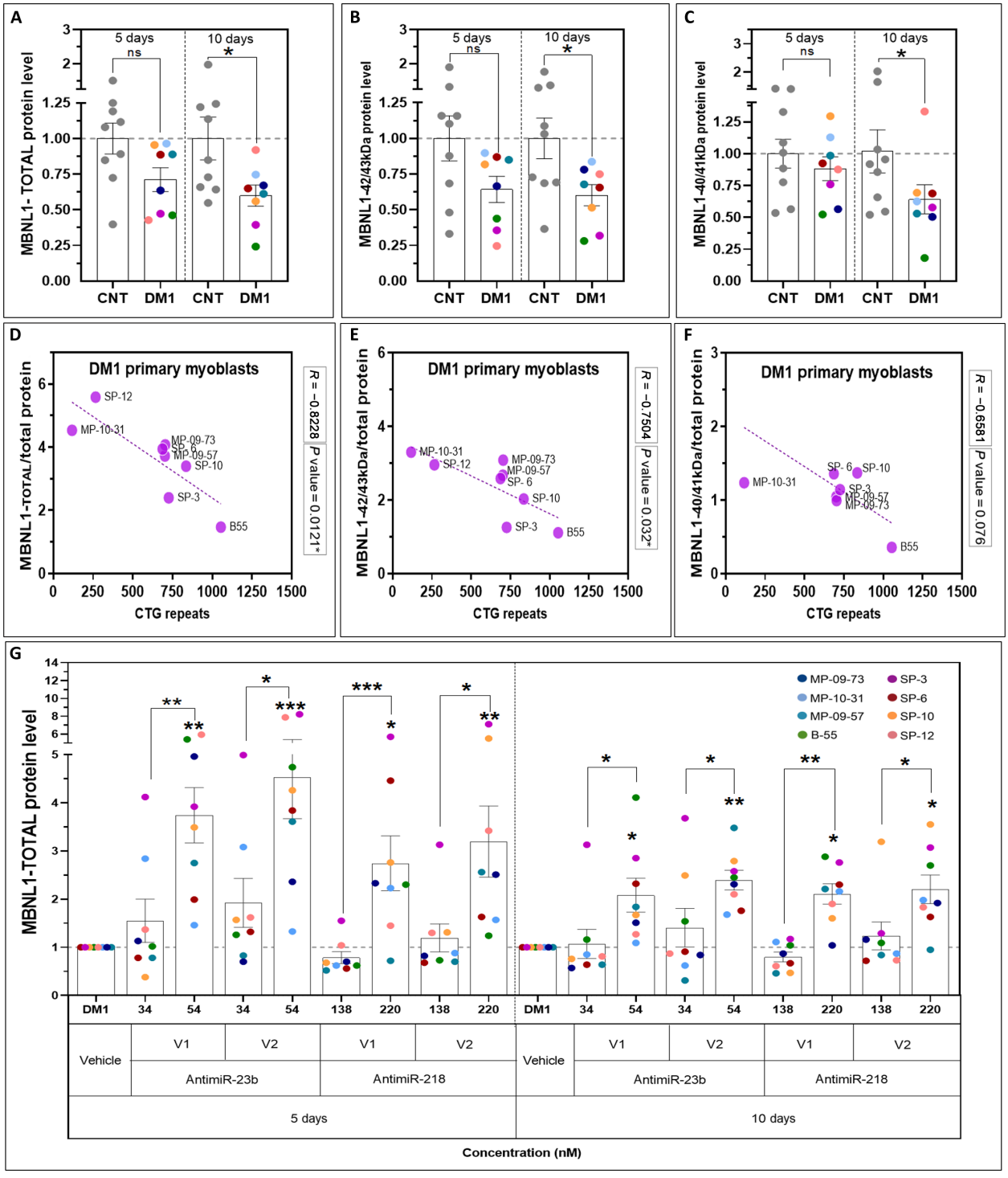

Fig. 2. Expression of MBNL1 proteins in DM1 cells and modulation by antimiR treatments. (**A** to **C**) Quantification of MBNL1 protein levels in control versus DM1 cells during differentiation. MBNL1 total protein levels (A) and for each isoform independently: MBNL1 42/43 kDa (+ex5 ±ex7) variant (B) and MBNL1 40/41 kDa (−ex5 ±ex7) variant (C) relative to the control condition of the same differentiation time. Unpaired *t* test. (**D** to **F**) Pearson correlation in untreated cells between MBNL1 protein levels normalized to the total protein and the number of CTG repetitions in DM1 myoblasts. CTG repeats versus MBNL1 total protein levels (D), MBNL1 42/43 kDa (+ex5 ±ex7) variant (E), and MBNL1 40/41 kDa (−ex5 ±ex7) variant (F). The correlation *R* value and *P* value are shown in the graph for each correlation. (**G**) Quantification of MBNL1 upon antimiR treatment relative to the nontreated DM1 condition. The asterisks above the bars denote DM1 comparisons, while those above the boxes denote dose comparisons. Kruskal-Wallis test $*P < 0.05$; $**P < 0.01$; $***P < 0.001$ (Dunn's posttest). Each dot of a different color denotes an individual DM1 myoblast line (shown in the legend). Error bars represent the SEM.

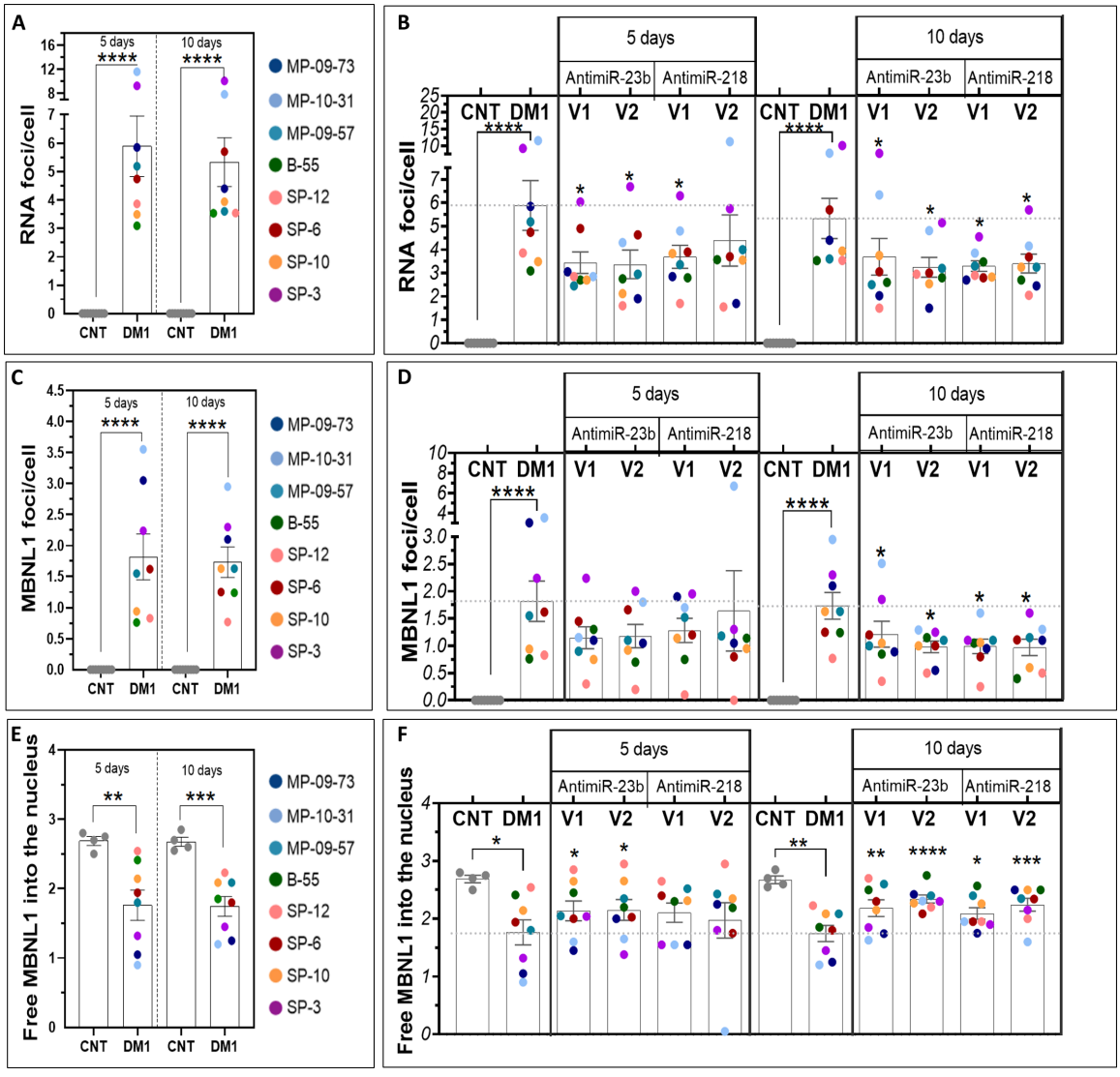

Fig. 3. Effect on foci number and cellular distribution of MBNL1. Number of (**A**) RNA nuclear foci per cell, (**C**) MBNL1 nuclear foci, and (**E**) MBNL1 free form in the nucleus in control versus DM1 cells during differentiation. Mann-Whitney test and unpaired *t* test with Welch's correction. In addition, the figure shows their responses to the indicated antimiR treatments (**B**, **D**, and **F**). Kruskal-Wallis test and two-way analysis of variance (ANOVA) **P* < 0.05; ***P* < 0.01; ****P* < 0.001; *****P* < 0.0001 (Dunn's posttest and Dunnett's posttest). Each dot of a different color denotes an individual DM1 myoblast line (shown in the legend). Error bars represent the SEM.

the number of foci in both time points, but a statistically significant difference was reached only after 10 days of differentiation. DM1 cells also presented an average of 1.7 to 2.0 MBNL1 nuclear foci (Fig. 3C) and a reduced presence of the protein as a diffused free-form in the nucleus (Fig. 3E), both indicative of functional sequestration of the protein. Both parameters were partially corrected upon antimiR treatment (Fig. 3, D and F), especially at the 10-day differentiation time point. As previously reported by others (*46*), we also detect more *DMPK* than MBNL1 nuclear foci in our primary myoblast cohort. While several technical issues could impinge on this result, particularly, higher sensitivity of RNA than protein detection because of lower background in the first than in the second case, it is also possible that expanded CUG transcripts go through several transient molecular stages inside the nucleus and show different protein binding capabilities. Representative images used for foci and MBNL1 quantification for all cell lines are shown in fig. S6, which also includes the use of an anti-human MBNL1 antibody to discard potential issues with the specific anti-mouse Mbnl1 epitope detected by MB1a (4A8).

At this point, we wondered about the reason behind the antimiR-mediated reduction of RNA and MBNL1 protein nuclear foci number. We analyzed *DMPK* expression in control and DM1 myoblasts to answer this question. We observed around 50% of normal *DMPK* expression in DM1 versus control cells after 5 days of differentiation, which went further down to 30% at the 10 days' time point (Fig. 4A). Our observation is in line with previous studies showing lower expression of *DMPK* expanded alleles (*47*, *48*), but *DMPK* relative expression only showed a trend toward correlating with CTG repeat size (Fig. 4B). AntimiR treatment induced a further reduction of *DMPK* levels in DM1 cells, particularly at the 10 days' time point, of

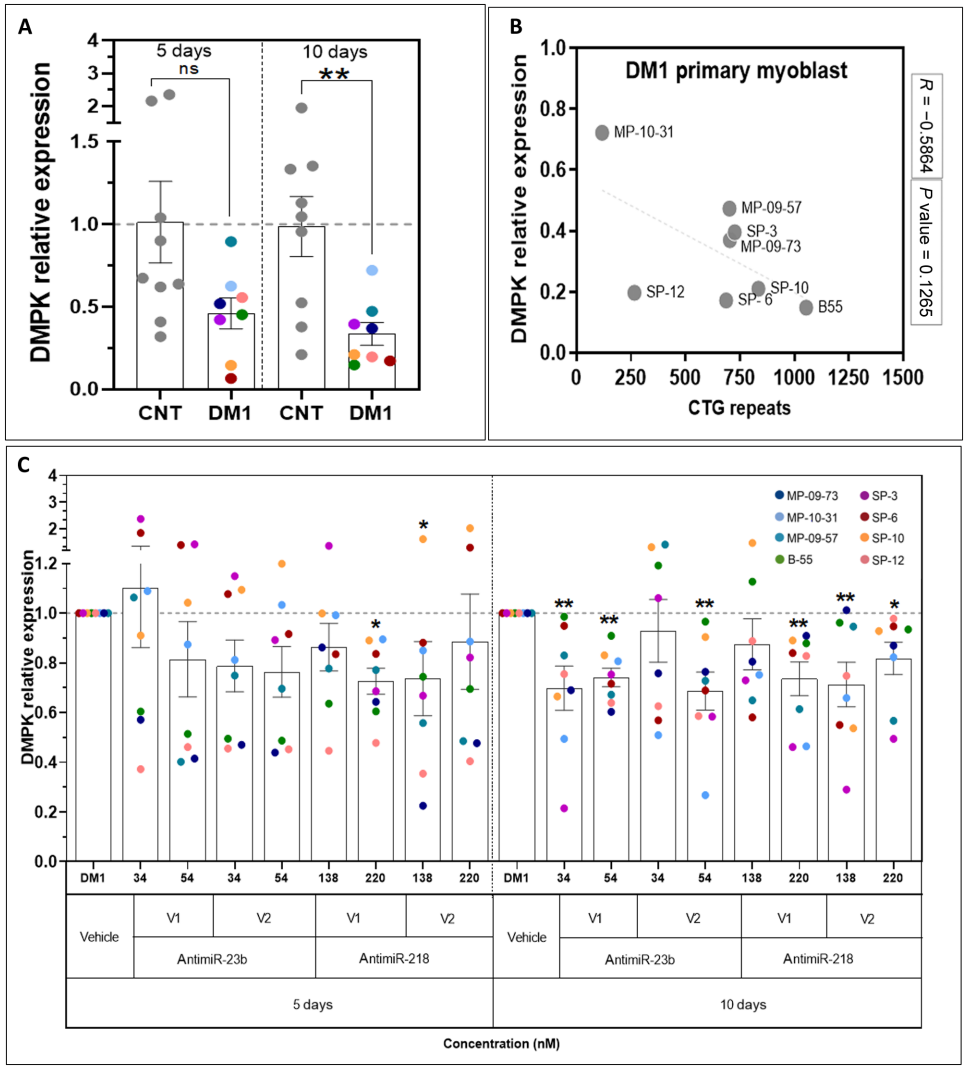

Fig. 4. Expression of *DMPK* mRNA in DM1 cells and treatment modulation. (**A**) Quantification of *DMPK* expression in control versus DM1 cells during differentiation. Mann-Whitney test and unpaired *t* test with Welch's correction. (**B**) Pearson correlation between *DMPK* expression levels and CTG repeat sizes in the cell lines. The correlation *R* value and *P* value are shown in the graph for each correlation (**C**) Quantification of *DMPK* expression upon antimiR treatments. Kruskal-Wallis test $*P < 0.05$; $**P < 0.01$ (Dunn's posttest). Each dot of a different color denotes an individual DM1 myoblast line (shown in the legend). Error bars represent the SEM.

up to ~25% (Fig. 4C). These results were reproduced with antimiR-23b-V1 and antimiR-23-V2 in immortalized DM1 muscle cells using a hot TRIzol protocol to ensure complete extractability of mutant *DMPK* transcripts (fig. S7A) and are consistent with previously published observations with the antimiR-218-V1 using the same cell line (*36*). Notably, cell lines that first reduced *DMPK* expression (at 5 days of differentiation) were those with a larger number of repeats, such as B55, MP-09-57, and MP-09-73, while lines showing a delayed response (at 10 days of differentiation) were those with smaller repeat sizes, such as MP-10-31 or SP-12. This suggests that the kinetics of *DMPK* degradation in response to antimiRs may depend on cellular cues, particularly repeat expansion size, but does not rule out that differences in basal *DMPK* gene expression or cellular compensation mechanisms among the cell lines used may also contribute to some cell lines responding earlier than others. Together, these data indicate that antimiR treatment successfully contributed to increasing the functional free-form levels of MBNL1 by increasing the protein expression and reducing the number of *DMPK* transcripts contributing to its sequestration.

When we analyzed these parameters' relationship with each cell line's disease load, we did not observe a significant correlation between the number of RNA or MBNL1 nuclear foci with CTG repeat length (fig. S7, B and C), which is consistent with the lack of relationship already observed between *DMPK* levels and repeat size (Fig. 4B). While to the extent of our knowledge, a correlation between foci number and disease severity has not been reported in the literature, we do detect a significant negative correlation between total MBNL1 protein and repeat expansion size (Fig. 2D). Last, we did observe a modest significant correlation between MBNL1 protein levels and the MBNL1 free into the nucleus, indicating a direct relationship between the increase of the protein and its availability as free form (fig. S7D). In sum, antimiRs rescue characteristic DM1 cellular alterations.

Correction of aberrant splicing in DM1 myoblasts

Next, we evaluated antimiRs on DM1 splicing defects at day 10 of differentiation because they generally show higher anti-DM1 disease activity than on day 5, and phenotypes are more clearly shown. With this purpose, we selected for validation by semiquantitative reverse transcription polymerase chain reaction (RT-PCR) experiments a panel of five genes whose splicing has been previously reported to be altered in DM1 skeletal muscle (*49*): *MBNL1* exon 5, *KIF13A* exon 26, *BIN1* exon 11, *SOS1* exon 21, and *PPFIBP1* exon 19 (fig. S8A). The quantification of exon inclusion from these genes revealed an ample window and significant difference between DM1 and control cells (Fig. 5A).

The splicing of *MBNL1* exon 5, *KIF13A* exon 26, *BIN1* exon 11, and *SOS1* exon 21 has been directly linked with a lack of MBNL1 activity in previous studies (*11, 43, 50, 51*). In addition, they correlate with force dorsiflexion in patients with DM1 (*50*). Notably, aberrant splicing of *BIN1*, a gene with crucial roles for muscle function (*52*), positively correlated with the patients' MIRS scale (fig. S8B; P value = 0.0815). In contrast, *PPFIBP1* exon 19 is not MBNL1 dependent (*53*), but it is also implicated in DM1 pathology, and its aberrant splicing can be rescued by the biguanide metformin, a drug that promotes corrective effects on several splicing defects associated with DM1 (*54*). We included this exon to verify whether antimiR treatment could contribute to its rescue independently of MBNL1 (e.g., through the down-regulation of *DMPK*).

Upon antimiR treatment, we observed an improved percentage of exon spliced-in ($\Delta PSI = PSI_{disease} - PSI_{treated}$), which was statistically significant for most alternative exons (Fig. 5B). In the case of *BIN1* exon 11, a significant correction was only reached with the higher doses of the antimiRs. For the rest of the alternative exons, both doses were effective. When looking at the overall ΔPSI that combined all exons analyzed (Fig. 5C), we observed a significant ~50% shift from the DM1 splicing pattern toward the control pattern for all antimiRs and doses used. ΔPSI values for each exon and treatment and gel images used for the quantification are depicted in fig. S9. We observed a moderate correlation of global ΔPSI scores with total MBNL1 protein levels (Fig. 5D, $P = 0.0005$, $R = 0.59$) and a low-to-moderate correlation for free MBNL1 form (Fig. 5E, $P = 0.0411$, $R = 0.37$), supporting a relationship between splicing correction and increased expression of total MBNL1 in cells treated with the antimiRs.

The correlation between overall ΔPSR scores and total MBNL1 protein levels was analyzed separately for miR-23b and miR-218 inhibition. The study found that samples using antimiR-23b-V1 and antimiR-23b-V2 showed a higher correlation compared to those using antimiR-218-V1 and antimiR-218-V2 (fig. S9, F and G).

We observed ~50% overall ΔPSI correction, with better rescues at the higher doses in MBNL1-dependent exons, consistent with the increased MBNL1 levels observed. Although all cell lines generally responded to treatment, 10-31 and SP-3 yielded somewhat lower splicing correction. Together, these results are consistent with the notion that only a moderate increase in MBNL1 is sufficient to achieve a therapeutic benefit and that antimiR treatment efficiently corrects downstream molecular DM1 alterations.

Functional rescue of myotubes area and fusion index

In previous studies, DM1 myoblasts have been shown to display defective differentiation compared to control cells, as determined by lower myotube area and fusion index (*55, 56*) . We analyzed both parameters in our DM1 primary myotubes and observed a strong reduction at days 5 and 10 of differentiation (Fig. 6, A and B). CTG repeat length only roughly correlated with decreased myotube area and fusion index (fig. S10, A and B). Representative images used for these quantifications are depicted in fig. S11A. We observed a negative correlation trend between the MIRS scale and myotube area (fig. S10C) but no correlation with the fusion index (fig. S10D). We had previously shown that miR-218 blockage alleviates fusion index upon differentiation of immortalized myoblasts (*36*) and miR-23b inhibition improved myotube area in a bioengineered in vitro three-dimensional (3D) model of DM1 (*57*). AntimiR treatment improved both parameters in primary DM1 cells (Fig. 6, C and D). AntimiR-23b-V2 managed to increase myotube area already at day 5 of differentiation and further improved this parameter by day 10 (Fig. 6C). Both antimiR-23b versions rescued the fusion index at the day 10 differentiation time point (Fig. 6D). In 2D cultures, the fusion index showed a significant correlation with myotube area ($P < 0.0001$; fig. S10E) in treated cells. Representative images of DM1 cells used for myotube area and fusion index quantification upon antimiR treatment are depicted in fig. S11B. These data support an improved ability for treated DM1 myoblasts with different genetic backgrounds and CTG expansions to differentiate into myotubes.

Integrated evaluation of the antimiR's therapeutic potential

To rank the preclinical potential of the antimiRs tested in this study, we evaluated the overall performance of the tested antimiRs. The four candidates were plotted in a spider graph comparing the degree of change (compared to control cells) in the five most important parameters previously evaluated: MBNL1 protein increase, RNA foci reduction, MBNL1 nuclear foci reduction, splicing recovery, and myotube differentiation recovery (Fig. 7A). This analysis suggested the selection of antimiR-23b-V2 as the lead candidate for further evaluation since it most consistently ranked at the top of these parameters, giving the largest area in the spider plot.

Focusing on antimiR-23b-V2, Fig. 7C shows not only the mean of DM1-derived myoblast lines more than doubled total MBNL1 levels compared to untreated but, importantly, that every single cell line responded to the antimiR despite unrelated genetic backgrounds and expansion sizes, which is indicative of a highly reliable in vitro effect. However, antimiR-23b-V2 potential to increase MBNL1 protein levels did not correlate significantly with CTG repeat size (Fig. 7B). Reduction of *DMPK* transcript levels followed a different behavior (Fig. 7, D and E) since three lines slightly increased *DMPK* mRNA levels with antimiR-23b-V2, while five reduced it, and lines with shorter expansions responded stronger, reducing *DMPK*. AntimiR-23b-V2 effect on overall splicing rescue was also remarkable since all lines responded to the treatment despite the fact that the antimiR activity in this parameter did not correlate with repeat size (Fig. 7, F and G). Last, the myotube area showed a significant repeat size–dependent rescue, and all individual lines improved (Fig. 7, H and I). Other parameters, such as MBNL1 quantification scale or fusion index, also revealed a general response by individual cell lines but did not seem to depend on CTG repeat number except for the fusion index response that was higher the lower the repeat size (fig. S12).

A notable controversy in the DM1 field involves the possibility that delayed differentiation issues could explain gene expression changes compared with control cells. While some studies describe normal myogenesis and increased apoptosis in primary DM1 muscle cells (*58*), others have reported myogenic defects in DM1 cell

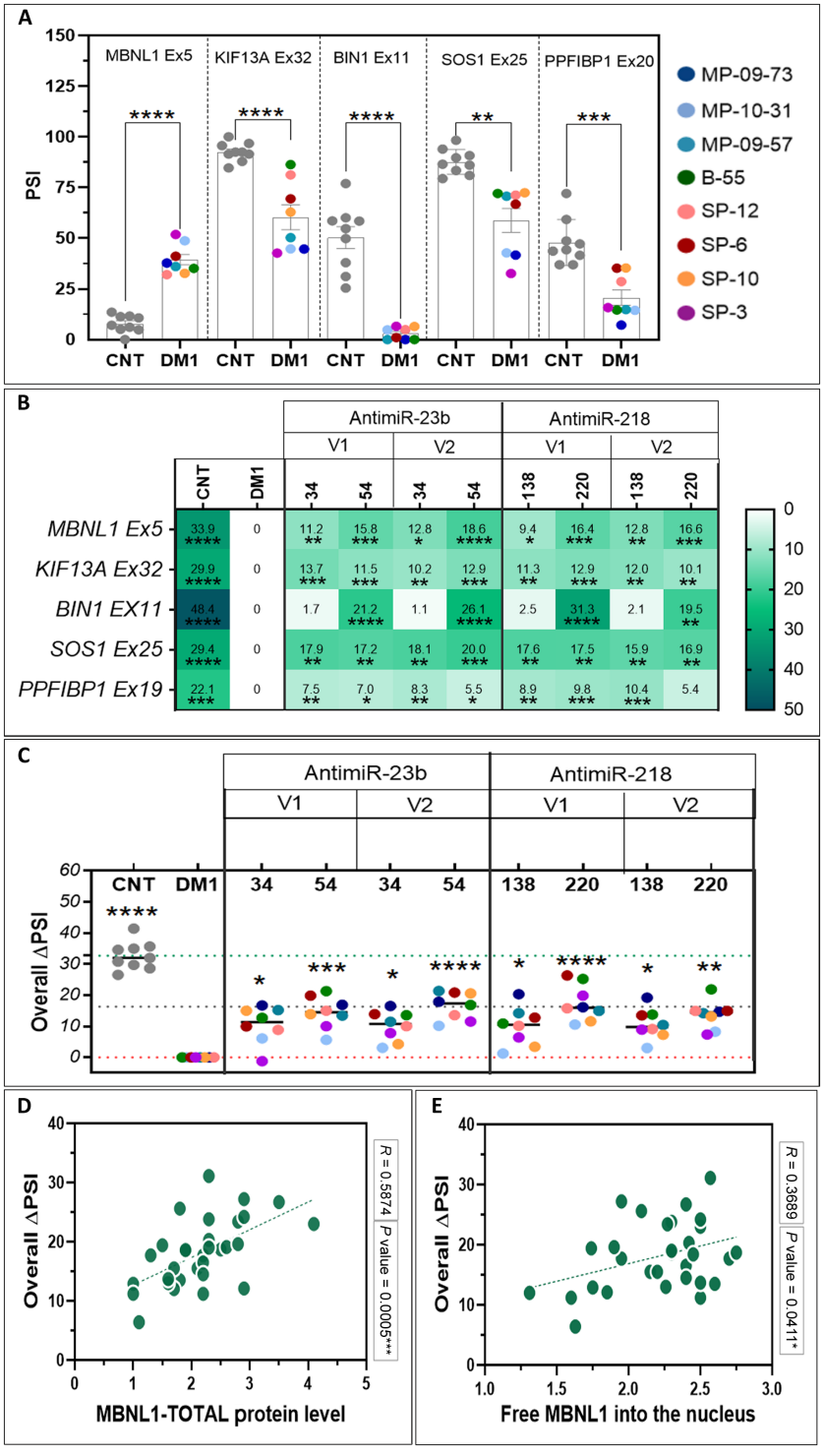

Fig. 5. Correction of DM1 splicing alterations. (**A**) Characterization of the percentage of spliced-in (PSI) in control versus DM1 cells for a selection of transcript exons. Unpaired *t* test and Mann-Whitney test. (**B**) Heatmap of the effect of antimiR treatment on the delta percentage of spliced-in (ΔPSI) of the indicated genes/exons. The numbers within the cells indicate the percentage changes in alternative exon inclusion between control and treated cells compared to untreated cells, which serve as the reference (change 0). The shading in the cells indicates the magnitude of the percentage change, with darker shades representing larger changes compared to the reference condition. (**C**) Overall correction of the ΔPSI per cell line. Kruskal-Wallis test $*P < 0.05$; $**P < 0.01$; $***P < 0.001$; $****P < 0.0001$ (Dunn's posttest). Each dot of a different color denotes an individual DM1 myoblast line (shown in the legend). Error bars represent the SEM. Pearson correlation between overall ΔPSI and total MBNL1 (**D**) and free form levels (**E**) in treated myotubes with the antimiRs. The correlation *R* value and *P* value are shown in the graph for each correlation.

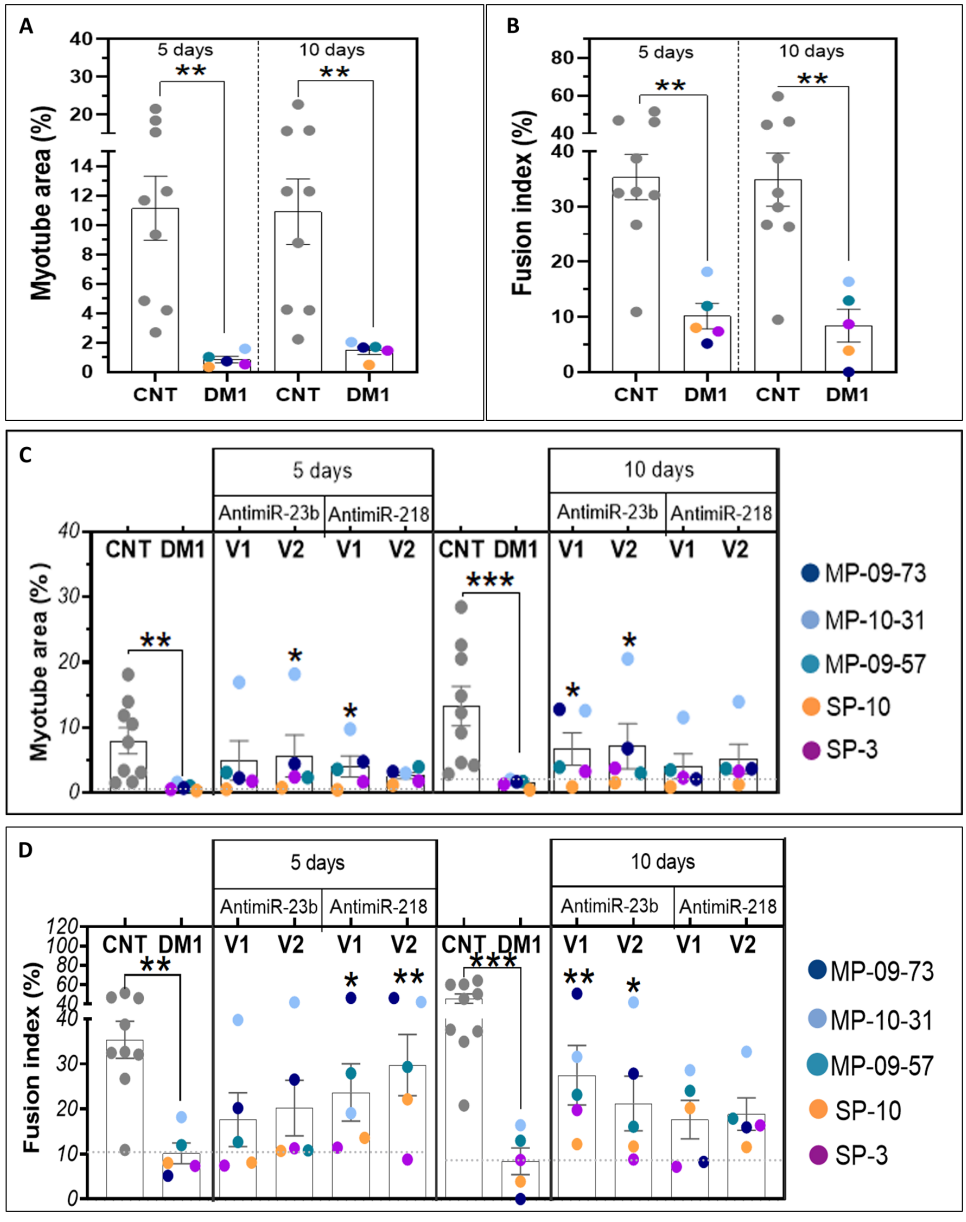

Fig. 6. Quantification of myotube area and fusion index in DM1 cells and treatment effect. Myotube area (**A**) and fusion index (**B**) quantifications are shown in control versus DM1 cells during differentiation. Unpaired *t* test with Welch's correction. Rescue of myotube area (**C**) and fusion index (**D**) upon treatment with the indicated antimiRs and conditions. Kruskal-Wallis test and two-way ANOVA $*P < 0.05$; $**P < 0.01$; $***P < 0.001$ (Dunn's posttest and Dunnett's posttest). Each dot of a different color denotes an individual DM1 myoblast line (shown in the legend).

models (*59*). To address this possibility, we have quantified miR-23b, MBNL1, and *DMPK* in healthy and DM1 cell lines before and at differentiation days 5 and 10, finding that compared to health controls, none of the gene expression changes can be explained as a delayed differentiation issue (fig. 13, A to C). Reduced MBNL1 levels during myogenesis in the presence of the expanded DM1 repeats were also consistent with previous reports (*44*). Also of interest is whether the repressive activity of miR-23b is active in a normal background or requires higher-than-normal miRNA levels. Figure S13 (D and E) shows that antimiR-23b-V2 can robustly antagonize miR-23b in a normal background, likely because of lower starting levels compared to DM1 and that this translates into up-regulated levels of MBNL1 protein as similarly observed in DM1 cells.

RNA-seq analysis of primary cells treated with antimiR-23b-V2

Next, we performed RNA sequencing (RNA-seq) experiments to test the effect on the transcriptome of our leading antimiR molecule. The depth of RNA-seq datasets was insufficient for a transcriptome-wide assessment, but this was already partially addressed by directly measuring five MBNL1-regulated alternative exons. We first analyzed the RNA samples of control versus DM1 myotubes at day 10 of differentiation

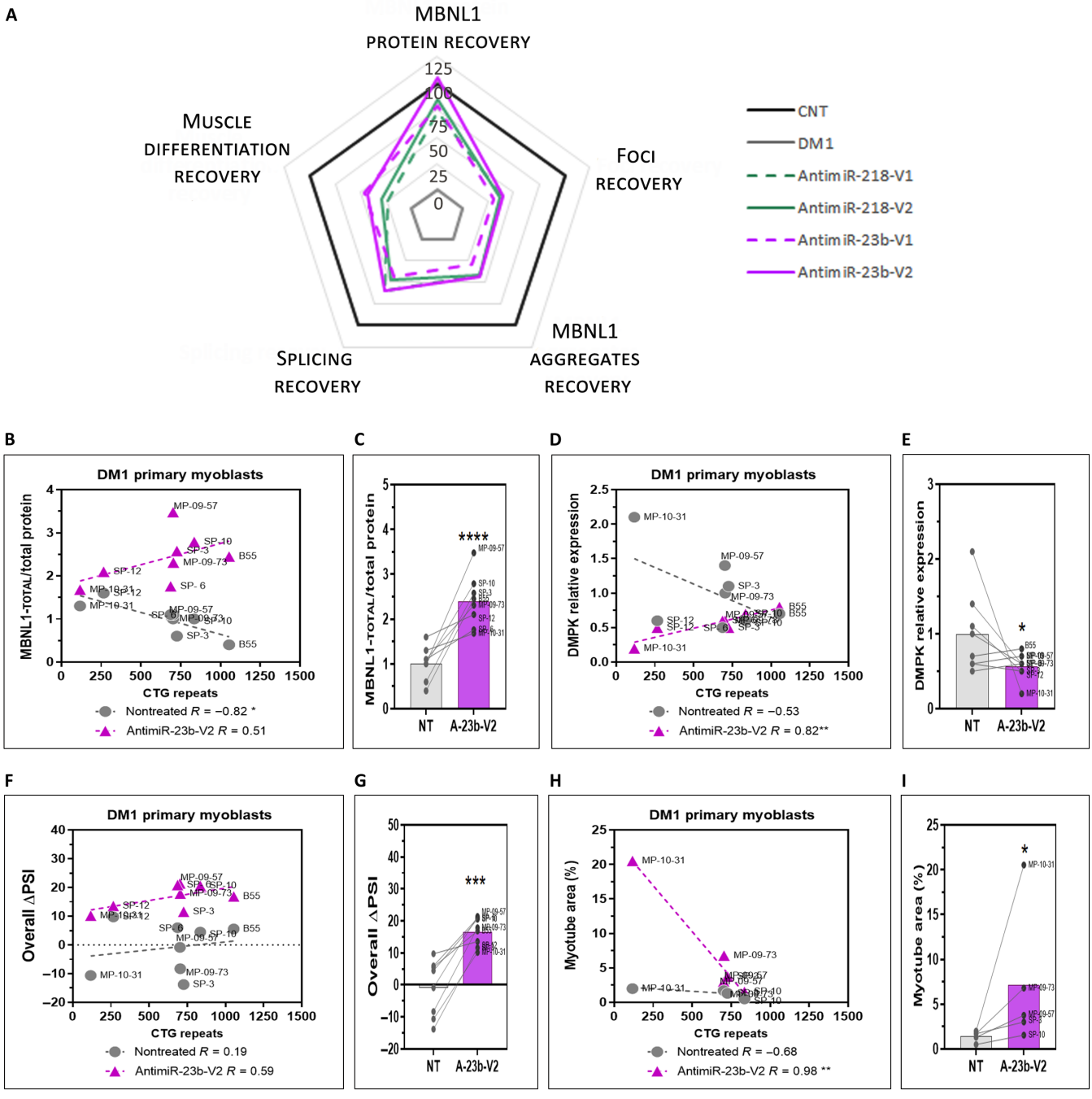

Fig. 7. Integrated evaluation of the antimiR's therapeutic potential. (**A**) Spider plot depicting the most relevant DM1 molecular readouts for each antimiR candidate. (**B** to **I**) Comparison of untreated DM1 myotubes with antimiR-23b-V2–treated DM1 myotubes, including the Pearson correlation with CTG repeat number, for the following parameters: [(B) and (C)] MBNL1 protein levels, [(D) and (E)] *DMPK* transcript levels, [(F) and (G)] overall ΔPSI, and [(H) and (I)] myotube area. Unpaired *t* test and Mann-Whitney test. *$P < 0.05$; **$P < 0.01$; ***$P < 0.001$; ****$P < 0.0001$. The correlation *R* values are shown in the corresponding graphs.

to identify disease-related genes (DRGs). This analysis revealed a total of 109 genes commonly dysregulated in all cell lines, 44 of which were down-regulated and 65 up-regulated (Fig. 8A). *TAF11L12*, *PRAMEF11*, *THBS4*, *MYH14*, and *AOC1* were the five most down-regulated genes, while *PRAME*, *THSD7B*, *SEMA3D*, *SNAP25*, and *CDH6* displayed the highest overexpression. To validate the clinical relevance of the detected DRGs, we crossed the list of 109 genes with publicly available RNA-seq data comparing tibialis muscle samples of patients with DM1 with controls (Fig. 8B). We observed a significant overlap of 29 genes ($P = 0.01$), proving that more than 25% of the DRGs detected in vitro are also deregulated in patient muscle biopsies. Then, we analyzed the change in the transcriptome of DM1 cells upon antimiR-23b-V2 treatment (Fig. 8C), detecting 42 and 44 genes significantly down-regulated and up-regulated, respectively. The $\log_2$ fold change ($\log_2$FC) magnitude of

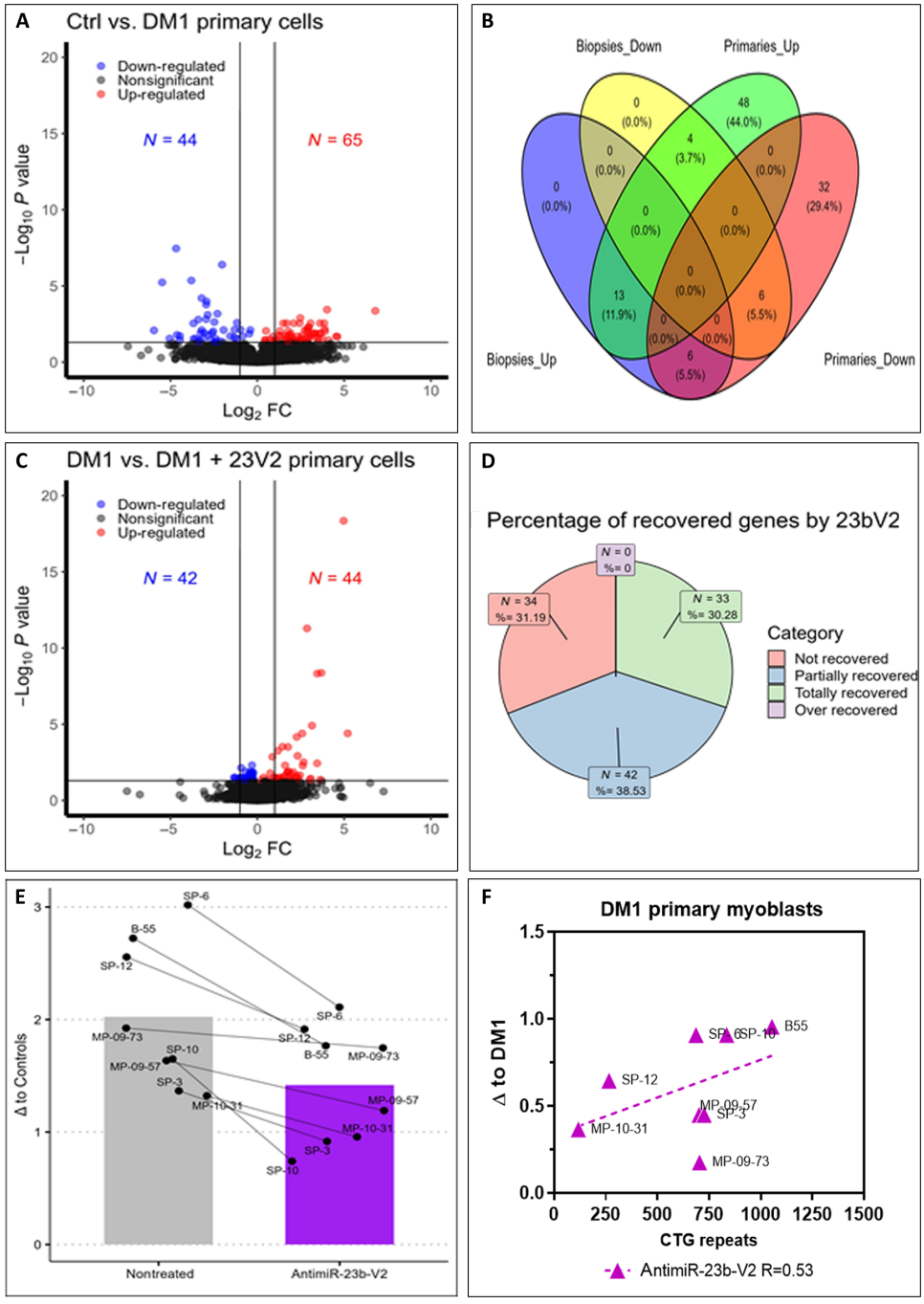

Fig. 8. RNA-seq analysis of primary myotubes after antimiR-23b-V2 treatment. (**A**) Volcano plot comparing the expression signature of untreated DM1 cells to control myotubes. (**B**) Overlap of DRGs found in the primary myotubes in vitro and genes dysregulated in the tibialis muscle of patients with DM1. (**C**) Volcano plot depicting the expression changes of DM1 cells upon antimiR-23b-V2 treatment. (**D**) Distribution of DRGs according to their change in expression upon antimiR-23b-V2, taking as reference the levels observed in control cells. (**E**) Average changes in DRG expression before and after antimiR-23b-V2 treatment (solid bars) and per cell line (connected dots) to highlight individual behaviors. (**F**) Linear regression between the overall change in DRG expression relative to DM1 and the number of CTG repeats in myotubes treated with antimiR-23b-V2. The correlation *R* values are displayed in the corresponding graphs.

down-regulated genes (mean $\log_2$FC of ~ −0.55) was low (i.e., close to untreated cells levels), while that of up-regulated genes was much more apparent (mean $\log_2$FC of ~3.8), where *HOXC12*, *THBS4*, *ZFP57*, *MYH14*, and *RPL29* pseudogene ranked among the top five. AntagomiR-23b-v2 was capable of increasing the expression of the *MYH14* gene, which had previously been reported to be decreased in DM1 (*60*). From the list of genes with expression changes upon antimiR-23b-V2 treatment, we calculated how many shifted toward the expression observed in control cells (Fig. 8D). We observed that the expression of 69% of the DRGs was partially or completely corrected by antimiR treatment. Last, we estimated the overall expression change of the DRGs upon antimiR-23b-V2 treatment for each cell line, finding that all primary myotubes

improved gene expression upon treatment (Fig. 8E), thus reinforcing the reliability of the therapeutic effect in genetically diverse DM1 cells. The largest changes in DRGs expression between untreated and antimiR-23 V-2–treated cells were found at the transcriptome level in cell lines with longer CTG repeats, like B55, showing a moderate correlation (Fig. 8F).

DISCUSSION

Our study in DM1 human-derived mature myotubes revealed that the most critical disease-associated molecular alterations could be reversed by blocking miR-23b and miR-218, two miRNAs that are natural repressors of MBNL1 (*34*). Transfection with antimiRs up-regulated this protein, alleviating main DM1 hallmarks such as foci number and *DMPK* expression, alternative missplicing, myotube area, and fusion index. Furthermore, as determined by RNA-seq, antimiR-23b-V2 reversed a substantial percentage of the common abnormal expression patterns observed in primary DM1 cells. All these molecular and cellular phenotypes have been previously confirmed in cell models of disease by independent studies (*55, 61–67*). Notably, total MBNL1 levels moderately correlated with splicing correction upon antimiR treatment (Fig. 5, D and E), consistent with a causal relationship.

Since DM1 is a highly heterogeneous disease, with variable degrees of clinical manifestations depending on CTG repeat size, our study using a diverse range of primary cells proves that antimiR treatment may successfully treat a broad spectrum of patients with DM1. In addition, on the basis of these results, we selected antimiR-23b-V2 for future preclinical development.

Previously, we reported that miR-218 was up-regulated in HSA^{LR} mice, DM1 cells, and muscle biopsies (*36*). In the present study, we extended these observations to primary mature myotubes. By 10 days in the differentiation medium, we found both miR-23b and miR-218 significantly up-regulated, consistent with the observed lowered amounts of total MBNL1 detected in untreated cells. Furthermore, estimated CTG repeat length in the cell lines significantly correlated with both miRNA levels, suggesting a shared pathological activation mechanism. From a therapeutic perspective, the fact that miR-218 and miR-23b are overexpressed in DM1 allows for a wider reduction window before reaching possible unwanted effects due to their complete inhibition. In this regard, loss of the miR-23b/27b/24-1 cluster impairs glucose tolerance in mice, noticeable after a high-fat diet induction (*68*). Thus, the combination of a higher-than-normal expression level of the therapeutic target miR-23b and lack of severe phenotypes, even with the complete removal of the miRNA in mice, makes it unlikely that a human antimiR-23b treatment may lead to significant detrimental effects as a DM1 therapy.

Prompted by the observation that antimiRs noticeably reduced ribonuclear foci in treated cells (Fig. 3B), we also quantified *DMPK* mRNA levels and found significant reductions (Fig. 4C). Compared to reports from actual clinical trials (*69*), this approximately 30% reduction in *DMPK* transcript levels in treated primary myoblasts is expected to have a clinically meaningful impact since smaller percentages of reduction from baseline (25%) already achieved a mean splicing correction of 13% across a panel of 22 genes and patients experienced a mean benefit of 3.8 s in myotonia after 6 months of administration. On top of this, antimiRs are expected to directly affect MBNL1 and 2 protein synthesis because of lowered amounts of repressive miR-23b and miR-218. Although our RT-qPCR assay cannot distinguish between normal and mutant *DMPK* transcripts, the fact that both the number of RNA and MBNL1 nuclear foci were strongly reduced suggests that at least a significant portion of expanded transcripts were reduced by antimiR treatment. In support of this hypothesis, non-expanded *DMPK* mRNAs are naturally exported to the cytoplasm and do not colocalize in the foci with MBNL1 proteins (*7*). Notably, independent studies reported the same phenomenon upon treatment with molecules not directly targeting *DMPK* (*70, 71*) but failed to explain it mechanistically. Correcting abnormal *MBNL1* exon 5 inclusion by antimiR treatment is expected to promote cytoplasmic MBNL1 levels [MBNL1 40/41; (*42, 72, 73*)], which is consistent with the confirmed change in the ratio between MBNL1 40/41 and MBNL1 42/43 in treated cells (fig. S5C). Since it has been previously shown that MBNL1 is the primary determinant of focus formation (*62*), by lowering the relative amount of MBNL1 in the nucleus, we hypothesize that foci may destabilize and originate the observed reduction of *DMPK* mRNA levels. In conclusion, because a direct interaction by the antimiRs with the *DMPK* RNA is unlikely due to minimal complementarity and MBNL1 has been shown to promote foci formation (*62*) and stability of nuclear *DMPK* (*74*), we hypothesize that the subcellular distribution of MBNL1 protein isoforms contributes to the destabilization of mutant *DMPK* mRNA, ultimately leading to the reduction of ribonuclear foci. Several other potential mechanisms, however, are also possible, such as an indirect effect through other RNA binding proteins involved in nuclear RNA stability and/or transport or *DMPK*-binding miRNAs, such as those proposed in (*75*) as potential binders to CUG repeat expansions. In addition, *DMPK* transcript reduction may explain why we observed correction of *PPFIBP1* exon 19 inclusion because this missplicing was reportedly altered in DM1 but independently of MBNL1 function (*53, 54*). Thus, any reduction in disease-causing *DMPK* levels is expected to rescue *PPFIBP1* splicing regardless of MBNL1 expression.

How antimiR molecules may reduce miRNA levels is a controversial issue as high-affinity antimiR chemistry has been shown to sequester the targeted miRNA in a heteroduplex, while lower-affinity oligonucleotides seem to promote miRNA degradation (*76*). However, the reduction in the levels may also be affected by competence between primer and antimiR annealing to the miRNA to be detected. Thus, reduction in the miRNA levels may be real or apparent, but in all cases, it is functionally relevant because the inability to amplify also confirms functional blockade. When comparing the ability of antimiRs against miR-23b or miR-218 to increase MBNL1 and reverse DM1-associated features, we obtained different results depending on the target. On the basis of previous experiments (*34*), we estimated that targeting miR-23b requires lower doses than those used for miR-218 to achieve comparable levels of MBNL1 up-regulation. In this study, we confirmed that lower doses (34 and 54 nM versus 138 and 220 nM) are sufficient to achieve therapeutic benefit in vitro using miR-23b–versus miR-218–targeting antimiRs, respectively. Compared to the previous versions (V1), our second-generation antimiRs (V2) incorporated PS backbone in the entire sequence, with a combination of 2′-OMe, MOE, and LNA residues, and were conjugated to a fatty acid instead of cholesterol. In addition, a side-by-side graphical comparison of desirable molecular and cellular rescues in DM1 reveals that V2 versions of antimiR-23b and -218 were superior to their V1 counterparts (Fig. 7A), used at the same concentration, in terms of the degree of MBNL1 up-regulation,

correction of alternative splicing, reduction of RNA and MBNL1 nuclear foci, and muscle differentiation markers (myotube area and fusion index). Overall, the improvement of antimiR-23b-V2 over antimiR-23b-V1 was greater than for the antimiR-218 counterparts.

The molecular response to antimiR-23b-V2 depended on CTG repeat sizes, and cell lines with small expansions showed significantly more pronounced *DMPK* mRNA reduction than those with longer repeats, while an inverse correlation was also significant for myotube area recovery. The reason why cell lines bearing small expansions reduced *DMPK* levels better than others may stem from the fact that they show higher basal MBNL1 levels compared to other DM1 lines (non-treated condition in Fig. 7B). Hence, as expected, cell lines with long repeats may require a higher increase in MBNL1 levels to get rid of *DMPK*, whereas cell lines with shorter repeats seem already closer to normal amounts, seemingly protective of *DMPK* accumulation. AntimiR-23b-V2's ability to enhance total MBNL1 levels and rescue splicing moderately ($R = 0.51$, and 0.59, respectively) correlated with CTG repeat size (Fig. 7, B and F).

Transcriptomics data analyses confirmed that treatment with antimiR-23b-V2 reversed the characteristic expression signature of DRGs that were dysregulated in primary DM1 myoblasts. These DM1-associated in vitro changes were representative (25%, $P = 0.01$) of gene expression alterations already reported in muscle biopsies (tibialis) of patients with DM1 (*49*), which is indicative of their therapeutic predictive power. Notably, individual analyses confirmed that all cell lines reduced the amount of dysregulated DRG upon antimiR-23b-V2 treatment, even with moderate increases in MBNL1 levels (~2 to 3-fold increases for all lines, Fig. 2G).

We propose a new model for the mechanism of action of antimiRs (fig. S14) in which the combined effect of blocking up-regulated miR-23b or miR-218 will derepress MBNL1 and other direct targets of these miRNAs and reduce *DMPK* transcript levels, leading to a synergistic correction of DM1 spliceopathy and related functional alterations. This poses a significant step forward in the preclinical validation of antimiRs together with previously demonstrated efficacy in vivo (*34*–*36*). To conclude, our study with antimiRs in a cohort of primary DM1 cell lines revealed that these molecules have therapeutic potential across unrelated genetic backgrounds. The approach works in cells with a wide range of repeats (range 117 to 1054), so it could be beneficial for treating multiple clinical forms of the disease.

MATERIALS AND METHODS

Study design

This study aimed to evaluate the therapeutic potential of candidate drugs antimiR-23b-V1, antimiR-218-V1, antimiR-23b-V2, and antimiR-218-V2 in human DM1 primary myoblasts of Table 1, which includes diverse ages, repeat sizes, and both sexes. The investigation involved analyzing DM1-related phenotypes such as fusion index, target miRNA levels, *DMPK* expression, ribonuclear foci number, MBNL1 nuclear foci and protein levels, and alternative splicing defects. Two differentiation time points (5 and 10 days) were evaluated. The concentrations used for antimiR-23b were 90 nM for immunocytochemistry (ICC) and fluorescent in situ hybridization (FISH) and 54 and 34 nM for protein and RNA analyses. The concentrations used for antimiR-218 were 366.7 nM for ICC and FISH studies and 220 and 138 nM for protein and RNA analyses. Myotubes for DNA, RNA, and protein analyses were collected as pellets, and coverslips were used for ICC and FISH assays at 5 and 10 days after differentiation and treatment (fig. S2). In addition, we conducted a thorough assessment of the therapeutic potential of the antimiRs and examined the individual responses of each cell line to antimiR-23b-V2. Furthermore, an RNA-seq experiment was carried out to investigate the impact of antimiR-23b-V2 on the transcriptome.

The sample sizes (n) are indicated in each figure, where each data point represents an individual cell line. Correlation analyses were performed to assess the degree of association between variables.

Sample donor characterization

A total of eight genetically confirmed patients with DM1 and nine controls with no personal or family history of neuromuscular diseases were included in the study. The essential clinical characterization of healthy and DM1 primary myoblast line donors is shown in Table 1 and was compiled from preexisting medical records from the indicated hospitals. Human samples used were collected following ethical guidelines and with appropriate study approval. The research was conducted following the ethical standards by the Comitè ética del Hospital Germans Trias i Pujol (cohort A), the Experimentation Ethics Committee of the University Hospital La Fe Valencia (cohort B), and Donostia University Hospital Ethical Board (cohort C), and the studies were approved under protocol numbers PI-15-009, 2014/0799, and 15-57, respectively. Informed consent was obtained from all participants or their legal guardians before sample collection. All procedures involving human samples adhered to the principles of the Declaration of Helsinki and relevant national regulations regarding the use of human subjects in research.

Primary myoblast isolation from muscle biopsy

Muscle biopsies were cleaned in a Ca^{2+}/Mg^{2+}–containing Hanks' balanced salt solution (Thermo Fisher Scientific) supplemented with 1% of penicillin-streptomycin and fungizone (amphotericin B; Thermo Fisher Scientific). Primary human myoblasts were isolated from the biopsied tissue by muscle explants and then purified by CD56 magnetic separation using CD56-coated microbeads (Miltenyi Biotec, Bergisch Gladbach, Germany) following the manufacturer's instructions.

CTG expansion sizing

DNA samples were extracted using the QIAamp DNA mini kit (Qiagen, Hilden, Germany). To determine CTG expansion size, an *Eco*RI digestion, followed by a long PCR and subsequent electrophoresis and Southern blot, was performed as described (*77*). The modal allele of each patient, which corresponds to the densest CTG bands, was estimated through comparison against the molecular weight ladder (GeneRuler 1-kb Plus Ladder, Thermo Fisher Scientific, Waltham, USA) using GelAnalyzer 19.1 software.

DMPK expression quantification by RT-qPCR

Total RNA was extracted using the miRNeasy Mini kit (Qiagen, #217004 and 79254), and 400 ng of RNA was converted to cDNA by random hexamer priming with SuperScript II (Invitrogen, #18064022), following the manufacturer's instructions. Subsequently, 0.2 ng cDNA was used with 5× HOT FIREPol Probe qPCR Mix Plus (Solis BioDyne, #08-01-00001) and PrimeTime qPCR (IDT, sequences shown table S1) probe assays for multiplex RT-qPCR on the QuantStudio 5 (Applied Biosystems; Foster City CA, USA). In the case of RNA isolated with Hot TRIzol from immortalized MyoD-inducible (doxycycline) DM1 fibroblasts (*55*), the protocol carried out was as described in Gagnon *et al.* (*78*). Relative expression of *DMPK* was measured and normalized to glyceraldehyde-3-phosphate dehydrogenase endogenous control,

relative to transfection reagent control samples, using the $2^{--\Delta\Delta Ct}$ methodology.

Protein extraction and Jess Simple Western

For total protein extraction, primary DM1 and control myotubes were disrupted by mechanical homogenization with an insulin syringe in Pierce radioimmunoprecipitation assay buffer (Thermo Fisher Scientific, #89901) supplemented with protease and phosphatase inhibitor cocktails (Roche Applied Science, #11836153001 and #4906837001) and subsequently sonicated. Total protein concentration was measured using a bicinchoninic acid protein assay kit (Thermo Fisher Scientific Pierce, # 23225) and bovine serum albumin as the protein standard.

The Jess Simple Western system was used to quantify MBNL1 protein from human primary myotubes, and measurements were normalized to total protein levels. Briefly, 1 μg of total protein from an individual experimental replicate (0.2 mg/ml) was separated in the Protein Normalization Assay module (ProteinSimple, Bio-Techne, # AM_PN01) and used to detect MBNL1 using a mouse anti-Mbnl1 primary antibody [MB1a (4A8), 1:10, MDA Monoclonal Antibody Resource (*7*)] and a goat horseradish peroxidase–conjugated anti-mouse immunoglobulin G secondary antibody (ProteinSimple, Bio-Techne, # DM-002). Chemiluminescent detection was performed using luminol-S and peroxide, following the manufacturer's instructions (ProteinSimple, Bio-Techne, # DM-002). Normalization was done through total protein chemiluminescence analysis (ProteinSimple, Bio-Techne, # RP-001) using the Total Protein Detection module (ProteinSimple, Bio-Techne, # DM-TP01). Total MBNL1 levels were defined as the sum of the previously described MBNL1 42/43 (+ex5 ± ex7) and MBNL1 40/41 (−ex5 ± ex7) variants (*44*), normalized to total loaded protein. For the individual expression of each isoform, each form was separately analyzed as MBNL1 42/43/loaded protein and MBNL1 42/43/loaded protein.

Statistical analyses

All statistical analyses were performed with Prism 8.2.1 (GraphPad). Results are presented as means ± SEM. An unpaired, two-tailed Student's *t* test was used for comparisons between two groups. A two-way analysis of variance (ANOVA) test was performed to compare various groups and conditions, followed by Dunnett's posttest. Where data did not follow normality, Kruskal-Wallis's test was applied followed by Dunn's posttest. Differences were considered significant at $P < 0.05$. Details about the statistical analysis used for each quantification are described in the corresponding figure legend. Sample sizes (n) are included in each figure, where each data point represents an individual cell line. Correlation analyses were carried out to measure the degree of association between two variables. In each case, the most appropriate correlation type, Pearson's or Sperman's, was used and is indicated in the figure legends. Correlation values were interpreted as very high (0.9 to 1), high (0.7 to 0.9), moderate (0.5 to 0.7), or low (0.3 to 0.5).

Supplementary Materials

This PDF file includes:

Supplementary Materials and Methods
Tables S1 and S2
Figs. S1 to S14
References

REFERENCES AND NOTES

1. J. D. Brook, M. E. McCurrach, H. G. Harley, A. J. Buckler, D. Church, H. Aburatani, K. Hunter, V. P. Stanton, J. P. Thirion, T. Hudson, R. Sohn, B. Zemelman, R. G. Snell, S. A. Rundle, S. Crow, J. Davies, P. Shelbourne, J. Buxton, C. Jones, V. Juvonen, K. Johnson, P. S. Harper, D. J. Shaw, D. E. Housman, Molecular basis of myotonic dystrophy: Expansion of a trinucleotide (CTG) repeat at the 3′ end of a transcript encoding a protein kinase family member. *Cell* **68**, 799–808 (1992).
2. T. Ashizawa, C. Gagnon, W. J. Groh, L. Gutmann, N. E. Johnson, G. Meola, R. Moxley III, S. Pandya, M. T. Rogers, E. Simpson, N. Angeard, G. Bassez, K. N. Berggren, D. Bhakta, M. Bozzali, A. Broderick, J. L. B. Byrne, C. Campbell, E. Cup, J. W. Day, E. De Mattia, D. Duboc, T. Duong, K. Eichinger, A.-B. Ekstrom, B. van Engelen, B. Esparis, B. Eymard, M. Ferschl, S. M. Gadalla, B. Gallais, T. Goodglick, C. Heatwole, J. Hilbert, V. Holland, M. Kierkegaard, W. J. Koopman, K. Lane, D. Maas, A. Mankodi, K. D. Mathews, D. G. Monckton, D. Moser, S. Nazarian, L. Nguyen, P. Nopoulos, R. Petty, J. Phetteplace, J. Puymirat, S. Raman, L. Richer, E. Roma, J. Sampson, V. Sansone, B. Schoser, L. Sterling, J. Statland, S. H. Subramony, C. Tian, C. Trujillo, G. Tomaselli, C. Turner, S. Venance, A. Verma, M. White, S. Winblad, Consensus-based care recommendations for adults with myotonic dystrophy type 1. *Neurol. Clin. Pract.* **8**, 507–520 (2018).
3. W. J. Groh, M. R. Groh, C. Shen, D. G. Monckton, C. L. Bodkin, R. M. Pascuzzi, Survival and CTG repeat expansion in adults with myotonic dystrophy type 1. *Muscle Nerve* **43**, 648–651 (2011).
4. M. De Antonio, C. Dogan, D. Hamroun, M. Mati, S. Zerrouki, B. Eymard, S. Katsahian, G. Bassez, Unravelling the myotonic dystrophy type 1 clinical spectrum: A systematic registry-based study with implications for disease classification. *Rev. Neurol.* **172**, 572–580 (2016).
5. C. Dogan, M. De Antonio, D. Hamroun, H. Varet, M. Fabbro, F. Rougier, K. Amarof, M. C. A. Bes, A.-L. Bedat-Millet, A. Behin, R. Bellance, F. Bouhour, C. Boutte, F. Boyer, E. Campana-Salort, F. Chapon, P. Cintas, C. Desnuelle, R. Deschamps, V. Drouin-Garraud, X. Ferrer, H. Gervais-Bernard, K. Ghorab, P. Laforet, A. Magot, L. Magy, D. Menard, M.-C. Minot, A. Nadaj-Pakleza, S. Pellieux, Y. Pereon, M. Preudhomme, J. Pouget, S. Sacconi, G. Sole, T. Stojkovich, V. Tiffreau, A. Urtizberea, C. Vial, F. Zagnoli, G. Caranhac, C. Bourlier, G. Riviere, A. Geille, R. K. Gherardi, B. Eymard, J. Puymirat, S. Katsahian, G. Bassez, Gender as a modifying factor influencing myotonic dystrophy type 1 phenotype severity and mortality: A nationwide multiple databases cross-sectional observational study. *PLOS One* **11**, e0148264 (2016).
6. L. L. Ozimski, M. Sabater-Arcis, A. Bargiela, R. Artero, The hallmarks of myotonic dystrophy type 1 muscle dysfunction. *Biol. Rev. Camb. Philos. Soc.* **96**, 716–730 (2021).
7. I. Holt, S. Mittal, D. Furling, G. S. Butler-Browne, J. D. Brook, G. E. Morris, Defective mRNA in myotonic dystrophy accumulates at the periphery of nuclear splicing speckles. *Genes Cells* **12**, 1035–1048 (2007).
8. E. S. Goers, J. Purcell, R. B. Voelker, D. P. Gates, J. A. Berglund, MBNL1 binds GC motifs embedded in pyrimidines to regulate alternative splicing. *Nucleic Acids Res.* **38**, 2467–2484 (2010).
9. R. Batra, K. Charizanis, M. Manchanda, A. Mohan, M. Li, D. J. Finn, M. Goodwin, C. Zhang, K. Sobczak, C. A. Thornton, M. S. Swanson, Loss of MBNL leads to disruption of developmentally regulated alternative polyadenylation in RNA-mediated disease. *Mol. Cell* **56**, 311–322 (2014).
10. X. Lin, J. W. Miller, A. Mankodi, R. N. Kanadia, Y. Yuan, R. T. Moxley, M. S. Swanson, C. A. Thornton, Failure of MBNL1-dependent post-natal splicing transitions in myotonic dystrophy. *Hum. Mol. Genet.* **15**, 2087–2097 (2006).
11. N. M. Kuyumcu-Martinez, G. S. Wang, T. A. Cooper, Increased steady-state levels of CUGBP1 in myotonic dystrophy 1 are due to PKC-mediated hyperphosphorylation. *Mol. Cell* **28**, 68–78 (2007).
12. A. Ravel-Chapuis, G. Bélanger, R. S. Yadava, M. S. Mahadevan, L. DesGroseillers, J. Côté, B. J. Jasmin, The RNA-binding protein Staufen1 is increased in DM1 skeletal muscle and promotes alternative pre-mRNA splicing. *J. Cell Biol.* **196**, 699–712 (2012).
13. M. Li, Y. Zhuang, R. Batra, J. D. Thomas, M. Li, C. A. Nutter, M. M. Scotti, H. A. Carter, Z. J. Wang, X. S. Huang, C. Q. Pu, M. S. Swanson, W. Xie, HNRNPA1-induced spliceopathy in a transgenic mouse model of myotonic dystrophy. *Proc. Natl. Acad. Sci. U.S.A.* **117**, 5472–5477 (2020).
14. F. Freyermuth, F. Rau, Y. Kokunai, T. Linke, C. Sellier, M. Nakamori, Y. Kino, L. Arandel, A. Jollet, C. Thibault, M. Philipps, S. Vicaire, B. Jost, B. Udd, J. W. Day, D. Duboc, K. Wahbi, T. Matsumura, H. Fujimura, H. Mochizuki, F. Deryckere, T. Kimura, N. Nukina, S. Ishiura, V. Lacroix, A. Campan-Fournier, V. Navratil, E. Chautard, D. Auboeuf, M. Horie, K. Imoto, K.-Y. Lee, M. S. Swanson, A. L. de Munain, S. Inada, H. Itoh, K. Nakazawa, T. Ashihara, E. Wang, T. Zimmer, D. Furling, M. P. Takahashi, N. Charlet-Berguerand, Splicing misregulation of SCN5A contributes to cardiac-conduction delay and heart arrhythmia in myotonic dystrophy. *Nat. Commun.* **7**, 11067 (2016).
15. T. M. Wheeler, J. D. Lueck, M. S. Swanson, R. T. Dirksen, C. A. Thornton, Correction of ClC-1 splicing eliminates chloride channelopathy and myotonia in mouse models of myotonic dystrophy. *J. Clin. Invest.* **117**, 3952–3957 (2007).
16. R. S. Savkur, A. V. Philips, T. A. Cooper, Aberrant regulation of insulin receptor alternative splicing is associated with insulin resistance in myotonic dystrophy. *Nat. Genet.* **29**, 40–47 (2001).
17. D. Savić Pavićević, J. Miladinović, M. Brkušanin, S. Šviković, S. Djurica, G. Brajušković, S. Romac, Molecular genetics and genetic testing in myotonic dystrophy type 1. *Biomed. Res. Int.* **2013**, 391821 (2013).

18. F. Morales, J. M. Couto, C. F. Higham, G. Hogg, P. Cuenca, C. Braida, R. H. Wilson, B. Adam, G. del Valle, R. Brian, M. Sittenfeld, T. Ashizawa, A. Wilcox, D. E. Wilcox, D. G. Monckton, Somatic instability of the expanded CTG triplet repeat in myotonic dystrophy type 1 is a heritable quantitative trait and modifier of disease severity. *Hum. Mol. Genet.* **21**, 3558–3567 (2012).
19. T. Ashizawa, J. R. Dubel, Y. Harati, Somatic instability of CTG repeat in myotonic dystrophy. *Neurology* **43**, 2674–2678 (1993).
20. C. A. Thornton, K. Johnson, R. T. Moxley III, Myotonic dystrophy patients have larger CTG expansions in skeletal muscle than in leukocytes. *Ann. Neurol.* **35**, 104–107 (1994).
21. M. Zatz, M. R. Passos-Bueno, A. Cerqueira, S. K. Marie, M. Vainzof, R. C. Pavanello, Analysis of the CTG repeat in skeletal muscle of young and adult myotonic dystrophy patients: When does the expansion occur? *Hum. Mol. Genet.* **4**, 401–406 (1995).
22. S. Peric, J. Pesovic, D. Savic-Pavicevic, V. Rakocevic Stojanovic, G. Meola, Molecular and clinical implications of variant repeats in myotonic dystrophy type 1. *Int. J. Mol. Sci.* **23**, 354 (2022).
23. M. Matloka, A. F. Klein, F. Rau, D. Furling, Cells of matter- *in vitro* models for myotonic dystrophy. *Front. Neurol.* **9**, 361 (2018).
24. M. Pascual-Gilabert, R. Artero, A. López-Castel, The myotonic dystrophy type 1 drug development pipeline: 2022 edition. *Drug Discov. Today* **28**, 103489 (2023).
25. S. J. Overby, E. Cerro-Herreros, B. Llamusi, R. Artero, RNA-mediated therapies in myotonic dystrophy. *Drug Discov. Today* **23**, 2013–2022 (2018).
26. P. Konieczny, E. Stepniak-Konieczna, K. Sobczak, MBNL proteins and their target RNAs, interaction and splicing regulation. *Nucleic Acids Res.* **42**, 10873–10887 (2014).
27. K. Charizanis, K.-Y. Lee, R. Batra, M. Goodwin, C. Zhang, Y. Yuan, L. Shiue, M. Cline, M. M. Scotti, G. Xia, A. Kumar, T. Ashizawa, H. B. Clark, T. Kimura, M. P. Takahashi, H. Fujimura, K. Jinnai, H. Yoshikawa, M. Gomes-Pereira, G. Gourdon, N. Sakai, S. Nishino, T. C. Foster, M. Ares Jr., R. B. Darnell, M. S. Swanson, Muscleblind-like 2-mediated alternative splicing in the developing brain and dysregulation in myotonic dystrophy. *Neuron* **75**, 437–450 (2012).
28. M. G. Poulos, R. Batra, M. Li, Y. Yuan, C. Zhang, R. B. Darnell, M. S. Swanson, Progressive impairment of muscle regeneration in muscleblind-like 3 isoform knockout mice. *Hum. Mol. Genet.* **22**, 3547–3558 (2013).
29. J. Choi, D. M. Dixon, W. Dansithong, W. F. Abdallah, K. P. Roos, M. C. Jordan, B. Trac, H. S. Lee, L. Comai, S. Reddy, Muscleblind-like 3 deficit results in a spectrum of age-associated pathologies observed in myotonic dystrophy. *Sci. Rep.* **6**, 30999 (2016).
30. C. M. Chamberlain, L. P. Ranum, Mouse model of muscleblind-like 1 overexpression: Skeletal muscle effects and therapeutic promise. *Hum. Mol. Genet.* **21**, 4645–4654 (2012).
31. K. Y. Song, X. M. Guo, H. Q. Wang, L. Zhang, S. Y. Huang, Y. C. Huo, G. Zhang, J. Z. Feng, R. R. Zhang, Y. Ma, Q. Z. Hu, X. Y. Qin, MBNL1 reverses the proliferation defect of skeletal muscle satellite cells in myotonic dystrophy type 1 by inhibiting autophagy via the mTOR pathway. *Cell Death Dis.* **11**, 545 (2020).
32. R. N. Kanadia, J. Shin, Y. Yuan, S. G. Beattie, T. M. Wheeler, C. A. Thornton, M. S. Swanson, Reversal of RNA missplicing and myotonia after muscleblind overexpression in a mouse poly(CUG) model for myotonic dystrophy. *Proc. Natl. Acad. Sci. U.S.A.* **103**, 11748–11753 (2006).
33. G. Chen, A. Masuda, H. Konishi, B. Ohkawara, M. Ito, M. Kinoshita, H. Kiyama, T. Matsuura, K. Ohno, Phenylbutazone induces expression of MBNL1 and suppresses formation of MBNL1-CUG RNA foci in a mouse model of myotonic dystrophy. *Sci. Rep.* **6**, 25317 (2016).
34. E. Cerro-Herreros, M. Sabater-Arcis, J. M. Fernandez-Costa, N. Moreno, M. Perez-Alonso, B. Llamusi, R. Artero, *miR-23b* and *miR-218* silencing increase muscleblind-like expression and alleviate myotonic dystrophy phenotypes in mammalian models. *Nat. Commun.* **9**, 2482 (2018).
35. E. Cerro-Herreros, I. González-Martínez, N. Moreno-Cervera, S. Overby, M. Pérez-Alonso, B. Llamusí, R. Artero, Therapeutic potential of antagomiR-23b for treating myotonic dystrophy. *Mol. Ther. Nucleic Acids* **21**, 837–849 (2020).
36. E. Cerro-Herreros, I. González-Martínez, N. Moreno, J. Espinosa-Espinosa, J. M. Fernández-Costa, A. Colom-Rodrigo, S. J. Overby, D. Seoane-Miraz, J. Poyatos-García, J. J. Vilchez, A. López de Munain, M. A. Varela, M. J. Wood, M. Pérez-Alonso, B. Llamusí, R. Artero, Preclinical characterization of antagomiR-218 as a potential treatment for myotonic dystrophy. *Mol. Ther. Nucleic Acids* **26**, 174–191 (2021).
37. S. Benizri, A. Gissot, A. Martin, B. Vialet, M. W. Grinstaff, P. Barthélémy, Bioconjugated oligonucleotides: Recent developments and therapeutic applications. *Bioconjug. Chem.* **30**, 366–383 (2019).
38. R. J. Butland, J. Pang, E. R. Gross, A. A. Woodcock, D. M. Geddes, Two-, six-, and 12-minute walking tests in respiratory disease. *Br. Med. J. Clin. Res. Ed* **284**, 1607–1608 (1982).
39. J. Mathieu, H. Boivin, D. Meunier, M. Gaudreault, P. Bégin, Assessment of a disease-specific muscular impairment rating scale in myotonic dystrophy. *Neurology* **56**, 336–340 (2001).
40. J. C. van Swieten, P. J. Koudstaal, M. C. Visser, H. J. Schouten, J. van Gijn, Interobserver agreement for the assessment of handicap in stroke patients. *Stroke* **19**, 604–607 (1988).
41. A. Compston, Aids to the investigation of peripheral nerve injuries. Medical Research Council: Nerve Injuries Research Committee. His Majesty's Stationery Office: 1942; pp. 48 (iii) and 74 figures and 7 diagrams; with aids to the examination of the peripheral nervous system. By Michael O'Brien for the Guarantors of Brain. Saunders Elsevier: 2010; pp. [8] 64 and 94 Figures. *Brain* **133**, 2838–2844 (2010).
42. H. Tran, N. Gourrier, C. Lemercier-Neuillet, C.-M. Dhaenens, A. Vautrin, F. J. Fernandez-Gomez, L. Arandel, C. Carpentier, H. Obriot, S. Eddarkaoui, L. Delattre, E. Van Brussels, I. Holt, G. E. Morris, B. Sablonnière, L. Buée, N. Charlet-Berguerand, S. Schraen-Maschke, D. Furling, I. Behm-Ansmant, C. Branlant, M.-L. Caillet-Boudin, N. Sergeant, Analysis of exonic regions involved in nuclear localization, splicing activity, and dimerization of muscleblind-like-1 isoforms. *J. Biol. Chem.* **286**, 16435–16446 (2011).
43. D. P. Gates, C. A. Coonrod, J. A. Berglund, Autoregulated splicing of muscleblind-like 1 (MBNL1) Pre-mRNA. *J. Biol. Chem.* **286**, 34224–34233 (2011).
44. L. M. André, R. T. P. van Cruchten, M. Willemse, D. G. Wansink, (CTG)n repeat-mediated dysregulation of MBNL1 and MBNL2 expression during myogenesis in DM1 occurs already at the myoblast stage. *PLOS One* **14**, e0217317 (2019).
45. A. Ballester-Lopez, J. Núñez-Manchón, E. Koehorst, I. Linares-Pardo, M. Almendrote, G. Lucente, N. Guanyabens, M. Lopez-Osias, A. Suárez-Mesa, S. A. Hanick, J. Chojnacki, A. Lucia, G. Pintos-Morell, J. Coll-Cantí, A. Martínez-Piñeiro, A. Ramos-Fransi, G. Nogales-Gadea, Three-dimensional imaging in myotonic dystrophy type 1: Linking molecular alterations with disease phenotype. *Neurol. Genet.* **6**, e484 (2020).
46. N. El Boujnouni, M. L. van der Bent, M. Willemse, P. A. C. 't Hoen, R. Brock, D. G. Wansink, Block or degrade? Balancing on- and off-target effects of antisense strategies against transcripts with expanded triplet repeats in DM1. *Mol. Ther. Nucleic Acids* **32**, 622–636 (2023).
47. S. Salvatori, M. Fanin, C. P. Trevisan, S. Furlan, S. Reddy, J. I. Nagy, C. Angelini, Decreased expression of DMPK: Correlation with CTG repeat expansion and fibre type composition in myotonic dystrophy type 1. *Neurol. Sci.* **26**, 235–242 (2005).
48. A. E. E. Gudde, I. D. G. van Kessel, L. M. André, B. Wieringa, D. G. Wansink, Trinucleotide-repeat expanded and normal DMPK transcripts contain unusually long poly(A) tails despite differential nuclear residence. *Biochim. Biophys. Acta Gene Regul. Mech.* **1860**, 740–749 (2017).
49. E. T. Wang, D. Treacy, K. Eichinger, A. Struck, J. Estabrook, H. Olafson, T. T. Wang, K. Bhatt, T. Westbrook, S. Sedehizadeh, A. Ward, J. Day, D. Brook, J. A. Berglund, T. Cooper, D. Housman, C. Thornton, C. Burge, Transcriptome alterations in myotonic dystrophy skeletal muscle and heart. *Hum. Mol. Genet.* **28**, 1312–1321 (2019).
50. M. Nakamori, K. Sobczak, A. Puwanant, S. Welle, K. Eichinger, S. Pandya, J. Dekdebrun, C. R. Heatwole, M. P. McDermott, T. Chen, M. Cline, R. Tawil, R. J. Osborne, T. M. Wheeler, M. S. Swanson, R. T. Moxley, C. A. Thornton, Splicing biomarkers of disease severity in myotonic dystrophy. *Ann. Neurol.* **74**, 862–872 (2013).
51. C. Fugier, A. F. Klein, C. Hammer, S. Vassilopoulos, Y. Ivarsson, A. Toussaint, V. Tosch, A. Vignaud, A. Ferry, N. Messaddeq, Y. Kokunai, R. Tsuburaya, P. de la Grange, D. Dembele, V. Francois, G. Precigout, C. Boulade-Ladame, M. C. Hummel, A. L. de Munain, N. Sergeant, A. Laquerrière, C. Thibault, F. Deryckere, D. Auboeuf, L. Garcia, P. Zimmermann, B. Udd, B. Schoser, M. P. Takahashi, I. Nishino, G. Bassez, J. Laporte, D. Furling, N. Charlet-Berguerand, Misregulated alternative splicing of BIN1 is associated with T tubule alterations and muscle weakness in myotonic dystrophy. *Nat. Med.* **17**, 720–725 (2011).
52. I. Prokic, B. S. Cowling, C. Kutchukian, C. Kretz, H. Tasfaout, V. Gache, J. Hergueux, O. Wendling, A. Ferry, A. Toussaint, C. Gavriilidis, V. Nattarayan, C. Koch, J. Lainé, R. Combe, L. Tiret, V. Jacquemond, F. Pilot-Storck, J. Laporte, Differential physiological roles for BIN1 isoforms in skeletal muscle development, function and regeneration. *Dis. Model Mech.* **13**, dmm044354 (2020).
53. M. Koshelev, S. Sarma, R. E. Price, X. H. Wehrens, T. A. Cooper, Heart-specific overexpression of CUGBP1 reproduces functional and molecular abnormalities of myotonic dystrophy type 1. *Hum. Mol. Genet.* **19**, 1066–1075 (2010).
54. D. Laustriat, J. Gide, L. Barrault, E. Chautard, C. Benoit, D. Auboeuf, A. Boland, C. Battail, F. Artiguenave, J. F. Deleuze, P. Bénit, P. Rustin, S. Franc, G. Charpentier, D. Furling, G. Bassez, X. Nissan, C. Martinat, M. Peschanski, S. Baghdoyan, In vitro and in vivo modulation of alternative splicing by the biguanide metformin. *Mol. Ther. Nucleic Acids* **4**, e262 (2015).
55. L. Arandel, M. Polay Espinoza, M. Matloka, A. Bazinet, D. De Dea Diniz, N. Naouar, F. Rau, A. Jollet, F. Edom-Vovard, K. Mamchaoui, M. Tarnopolsky, J. Puymirat, C. Battail, A. Boland, J. F. Deleuze, V. Mouly, A. F. Klein, D. Furling, Immortalized human myotonic dystrophy muscle cell lines to assess therapeutic compounds. *Dis. Model. Mech.* **10**, 487–497 (2017).
56. M. Sabater-Arcis, A. Bargiela, N. Moreno, J. Poyatos-Garcia, J. J. Vilchez, R. Artero, Musashi-2 contributes to myotonic dystrophy muscle dysfunction by promoting excessive autophagy through *miR-7* biogenesis repression. *Mol. Ther. Nucleic Acids* **25**, 652–667 (2021).
57. X. Fernández-Garibay, M. A. Ortega, E. Cerro-Herreros, J. Comelles, E. Martínez, R. Artero, J. M. Fernández-Costa, J. Ramón-Azcón, Bioengineered *in vitro* 3D model of myotonic dystrophy type 1 human skeletal muscle. *Biofabrication* **13**, 035035 (2021).

58. E. Loro, F. Rinaldi, A. Malena, E. Masiero, G. Novelli, C. Angelini, V. Romeo, M. Sandri, A. Botta, L. Vergani, Normal myogenesis and increased apoptosis in myotonic dystrophy type-1 muscle cells. *Cell Death Differ.* **17**, 1315–1324 (2010).
59. J. D. Amack, M. S. Mahadevan, Myogenic defects in myotonic dystrophy. *Dev. Biol.* **265**, 294–301 (2004).
60. F. Rinaldi, C. Terracciano, V. Pisani, R. Massa, E. Loro, L. Vergani, S. Di Girolamo, C. Angelini, G. Gourdon, G. Novelli, A. Botta, Aberrant splicing and expression of the non muscle myosin heavy-chain gene MYH14 in DM1 muscle tissues. *Neurobiol. Dis.* **45**, 264–271 (2012).
61. D. Furling, L. Coiffier, V. Mouly, J. P. Barbet, J. L. S. Guily, K. Taneja, G. Gourdon, C. Junien, G. S. Butler-Browne, Defective satellite cells in congenital myotonic dystrophy. *Hum. Mol. Genet.* **10**, 2079–2087 (2001).
62. W. Dansithong, S. Paul, L. Comai, S. Reddy, MBNL1 is the primary determinant of focus formation and aberrant insulin receptor splicing in DM1. *J. Biol. Chem.* **280**, 5773–5780 (2005).
63. A. Bigot, A. F. Klein, E. Gasnier, V. Jacquemin, P. Ravassard, G. Butler-Browne, V. Mouly, D. Furling, Large CTG repeats trigger p16-dependent premature senescence in myotonic dystrophy type 1 muscle precursor cells. *Am. J. Pathol.* **174**, 1435–1442 (2009).
64. V. François, A. F. Klein, C. Beley, A. Jollet, C. Lemercier, L. Garcia, D. Furling, Selective silencing of mutated mRNAs in DM1 by using modified hU7-snRNAs. *Nat. Struct. Mol. Biol.* **18**, 85–87 (2011).
65. A. Botta, A. Malena, E. Loro, G. Del Moro, M. Suman, B. Pantic, G. Szabadkai, L. Vergani, Altered Ca^{2+} homeostasis and endoplasmic reticulum stress in myotonic dystrophy type 1 muscle cells. *Genes* **4**, 275–292 (2013).
66. M. Sabater-Arcis, A. Bargiela, D. Furling, R. Artero, miR-7 restores phenotypes in myotonic dystrophy muscle cells by repressing hyperactivated autophagy. *Mol. Ther. Nucleic Acids* **19**, 278–292 (2020).
67. V. Todorow, S. Hintze, A. R. W. Kerr, A. Hehr, B. Schoser, P. Meinke, Transcriptome analysis in a primary human muscle cell differentiation model for myotonic dystrophy type 1. *Int. J. Mol. Sci.* **22**, 8607 (2021).
68. Y.-H. Jiang, Y.-Y. Man, Y. Liu, C.-J. Yin, J.-L. Li, H.-C. Shi, H. Zhao, S.-G. Zhao, Loss of miR-23b/27b/24-1 cluster impairs glucose tolerance via glycolysis pathway in mice. *Int. J. Mol. Sci.* **22**, 550 (2021).
69. Dyne Therapeutics Announces Positive Initial Clinical Data from ACHIEVE Trial in DM1 Patients and DELIVER Trial in DMD Patients Demonstrating Promise of the FORCE™ Platform in Developing Therapeutics for Rare Muscle Diseases | Dyne Therapeutics, Inc. https://investors.dyne-tx.com/news-releases/news-release-details/dyne-therapeutics-announces-positive-initial-clinical-data/.
70. M. Wang, W.-C. Weng, L. Stock, D. Lindquist, A. Martinez, G. Gourdon, N. Timchenko, M. Snape, L. Timchenko, Correction of glycogen synthase kinase 3β in myotonic dystrophy 1 reduces the mutant RNA and improves postnatal survival of DMSXL mice. *Mol. Cell. Biol.* **39**, e00155-19 (2019).
71. L. Witherspoon, S. O'Reilly, J. Hadwen, N. Tasnim, A. MacKenzie, F. Farooq, Sodium channel inhibitors reduce DMPK mRNA and protein. *Clin. Transl. Sci.* **8**, 298–304 (2015).
72. Y. Kino, C. Washizu, M. Kurosawa, Y. Oma, N. Hattori, S. Ishiura, N. Nukina, Nuclear localization of MBNL1: Splicing-mediated autoregulation and repression of repeat-derived aberrant proteins. *Hum. Mol. Genet.* **24**, 740–756 (2015).
73. F. Terenzi, A. N. Ladd, Conserved developmental alternative splicing of muscleblind-like (MBNL) transcripts regulates MBNL localization and activity. *RNA Biol.* **7**, 43–55 (2010).
74. X. Xing, R. Markus, T. Ghosh, S. Buxton, D. J. Nieves, M. Wojciechowska, J. D. Brook, Regulation of Toxic RNA Foci and Mutant DMPK Transcripts: Role of MBNL Proteins and RNA Decay Pathways. bioRxiv [Preprint] (2023). https://doi.org/10.1101/2023.09.28.559487.
75. E. Koscianska, T. M. Witkos, E. Kozlowska, M. Wojciechowska, W. J. Krzyzosiak, Cooperation meets competition in microRNA-mediated DMPK transcript regulation. *Nucleic Acids Res.* **43**, 9500–9518 (2015).
76. J. Stenvang, A. Petri, M. Lindow, S. Obad, S. Kauppinen, Inhibition of microRNA function by antimiR oligonucleotides. *Silence* **3**, 1 (2012).
77. E. Koehorst, J. Núñez-Manchón, A. Ballester-López, M. Almendrote, G. Lucente, A. Arbex, J. Chojnacki, R. P. Vázquez-Manrique, A. P. Gómez-Escribano, G. Pintos-Morell, J. Coll-Cantí, A. Ramos-Fransi, A. Martínez-Piñeiro, M. Suelves, G. Nogales-Gadea, Characterization of RAN translation and antisense transcription in primary cell cultures of patients with myotonic dystrophy type 1. *J. Clin. Med.* **10**, 5520 (2021).
78. K. T. Gagnon, L. Li, B. A. Janowski, D. R. Corey, Analysis of nuclear RNA interference in human cells by subcellular fractionation and Argonaute loading. *Nat. Protoc.* **9**, 2045–2060 (2014).
79. K.-T. Lin, A. R. Krainer, PSI-Sigma: A comprehensive splicing-detection method for short-read and long-read RNA-seq analysis. *Bioinformatics* **35**, 5048–5054 (2019).

Acknowledgments: Antibody MB1a (4A8) was provided by MDA Monoclonal Antibody Resources. We acknowledge the service of Medical Science Consulting (Valencia, Spain) for scientific writing support. Part of the equipment employed in this work has been funded by Generalitat Valenciana and cofinanced with ERDF funds (OP ERDF of Comunitat Valenciana 2014-2020). **Funding:** This work was financially supported by the following: "la Caixa" Banking Foundation grant HR17-00268 (R.A.), Generalitat Valenciana grant PROMETEO/2020/081 (R.A), Instituto de Salud Carlos III grant PI22/00104 (G.N.-G.), AFM-Telethon grant #24757 (G.N.-G.), Ministerio de Ciencia e Innovación grant CNS2022-135519 (G.N.-G.), Ministerio de Ciencia e Innovación grant PID2020-118730RB-I00 (M.S.), Generalitat Valenciana post-doctoral fellowship APOSTD/2019/142 (E.C.-H.), Generalitat Valenciana predoctoral fellowship FDEGENT/2020/001 (I.G.-M.), Instituto de Salud Carlos III I-PFIS fellowship grant IFI20/00022 (J.N.-M.), Headstart of Eit Health (EU), project "ARTHEx-DM1" (2020-HS-0215) (B.L.), CDTI NEOTEC grant SNEO-20201136 (B.L.), GVA-IVACE grant IMIDTA/2021/65) (B.L.), and Torres Quevedo post-doctoral fellowship PTQ2020-011110 (E.C.-H.). Additional funding was from the project "DISMIOTATX" with reference CPP2022-009960, funded by MCIN/AEI/10.13039/501100011033 and, as appropriate, by the "European Union NextGenerationEU/PRTR" to (B.L, G.N.-G., and R.A).
Author contributions: Data curation: J.E.-E. Conceptualization: E.C.-H., G.N.-G., B.L., and R.A. Methodology: E.C.-H., J.N.-M., M.C.-S., A.G.-R., M.S., G.N.-G., and B.L. Investigation: E.C.-H., J.N.-M., N.N.-G., M.C.-S., A.G.-R., D.P.L., K.M., and J.P.-G. Validation: E.C.H., A.G.-R., and D.P.L. Visualization: E.C.-H., M.C.-S., A.G.-R., and D.P.L. Supervision: E.C.-H., A.L.d.M., B.L., and R.A. Writing—original draft: E.C.-H., J.N.-M., and A.G.-R. Writing—review and editing: E.C.-H., J.J.-V., G.N.-G., B.L., and R.A. Resources: J.P.-G., J.J.V., A.L.d.M., M.S., G.N.-G., and B.L. Project administration: B.L. and R.A. Formal analysis: E.C.-H., A.G.-R., I.G.-M., and J.E.-E. Funding acquisition: B.L., G.N.-G., M.S., and R.A. **Competing interests:** B.L. and R.A. are founders and CEO and scientific advisor of Arthex Biotech, respectively. B.L., E.C.-H., and R.A. are coinventors on patents PCT/EP2017/073685 and EP22382493, currently licensed to Arthex Biotech. The remaining authors declare that they have no competing interests. **Data and materials availability:** All materials used in this study are available upon reasonable request. Access to the antimiRs can be arranged by Arthex Biotech pending scientific review and a completed material transfer agreement. Genomic and TCR sequencing data are available at the Gene Expression Omnibus website (accession number GSE237411). All data needed to evaluate the conclusions in the paper are present in the paper and/or the Supplementary Materials.

Submitted 20 December 2023
Accepted 5 September 2024
Published 9 October 2024
10.1126/sciadv.adn6525